NASA Contractor Report 178312

Simulation of Automatic Precision Departures and Missed Approaches Using the Microwave Landing System

J. B. Feather

McDonnell Douglas Corporation
Long Beach, California 90846

Contract NAS1-16202
July 1987

National Aeronautics and
Space Administration

Langley Research Center
Hampton, Virginia 23665-5225

NASA Contractor Report 178312

Simulation of Automatic Precision Departures and Missed Approaches Using the Microwave Landing System

J. B. Feather

McDonnell Douglas Corporation
Long Beach, California 90846

Contract NAS1-16202
July 1987

National Aeronautics and
Space Administration

Langley Research Center
Hampton, Virginia 23665-5225

TABLE OF CONTENTS

TABLE OF CONTENTS
(continued)

TABLE OF CONTENTS
(continued)

LIST OF FIGURES

LIST OF FIGURES
(continued)

PAGE

LIST OF FIGURES
(continued)

LIST OF FIGURES
(continued)

PAGE

LIST OF TABLES

LIST OF SYMBOLS

b	Factor used in back azimuth coordinate derivation, non dimensional (ND)
c	Factor used in back azimuth coordinate derivation
h	Altitude, ft.
R_{DME}	Range from DME/P transmitter to MLS aircraft antenna, ft.
S_x, S_y, S_z	Wind magnitude at 33 ft. altitude in earth coordinates, KT
u_g, v_g, w_g	Turbulence levels along x-y-z axes, KT
W	Wind factor as a function of altitude, ND
WP	Waypoint identifier, ND
W_X, W_Y, W_Z	Wind magnitudes at altitude h in earth coordinates, KT
$W_{TX}, W_{TY} W_{TZ}$	Total winds (including turbulence), KT
x, y, h	Coordinates of a given waypoint, ft.
x'_m, y'_m, z'_m	Coordinates defining MLS antenna location, ft.
x_m, y_m, z_m	Coordinates of CG location, ft.
x_B	Distance from coordinate origin to the DME/P and front azimuth transmitters, ft.
x_D	Distance from coordinate origin to the back azimuth transmitter, ft.
θ_{AZ}	MLS azimuth angle, deg.
θ_{BAZ}	MSL back azimuth angle, deg.

θ_{CE}	Pitch steering command, deg.
θ_{EL}	MLS elevation angle, deg.
σ	Standard deviation used in turbulence filter, KT.
σ_{REC}	Standard deviation at MLS receiver output, deg
σ_{WN}	White noise gain factor, ND
τ	Time constant, sec.
ω_h	High frequency MLS noise filter parameter, rad/sec
ω_ℓ	Low frequency MLS noise filter parameter, rad/sec

SUMMARY AND INTRODUCTION

Results of studies in which precision departures and missed approaches were simulated using MLS guidance techniques are presented in this report. The study was conducted under the Terminal Configured Vehicle (TVC) Program, and is an extension of a previous NASA Advanced Transport Operating Systems (ATOPS) contract, NAS1-18028, (Reference 1) in which complex approach paths were evaluated. Simulation of precision departures using MLS back azimuth coverage has provided additional performance data. In addition, missed approaches, which include transitioning from front MLS coverage to back azimuth operation, have been simulated. For purposes of this simulation, the elevation antenna used for front MLS coverage has been located on the runway centerline. In practice, this antenna will be displaced laterally, so the resulting equations for the aircraft position coordinates will be somewhat more complicated than those assumed in this study.

As in the previous studies, an MD-80 aircraft was simulated using its present roll and pitch autopilot inner loop configurations. The outer loops consisted of inputs from the MLS guidance algorithms that provided the roll and pitch steering commands. With only minor changes, these algorithms are the same as those previously developed (References 1 and 2). This simulation implemented the MLS guidance laws in conjunction with the MD-80 take off and go around pitch autopilot modes. For departures, the pitch guidance was the normal take off mode, whereas the lateral guidance was under MLS curved path control. For missed approaches, normal MLS vertical and lateral approach guidance was used prior to go around initiation. At that time, the pitch autopilot was changed to go around mode, and the lateral guidance remained in its approach mode. Switching to MLS back azimuth mode occurred when the aircraft first passed into back azimuth coverage. For missed approaches, no lateral maneuvers were simulated.

This effort consisted of departures and missed approaches at an airport where MLS, when installed, would provide an operational benefit. MLS would allow noise abatement take off procedures which otherwise would not be possible due to weather constraints. Several noise abatement departure paths were simulated and included the effects of MLS noise, winds, and turbulence on performance. Two missed approach procedures were simulated to assess the vertical and lateral path tracking accuracies of the system.

CONCLUSIONS AND RECOMMENDATIONS

CONCLUSIONS

Generally, the simulated precision departures for the MD-80 provided acceptable lateral tracking performance, except in cases where bank angles led to operation near autopilot inner loop command limits. In those cases, tracking errors up to 1500 feet occurred, and the lateral guidance system was not capable of controlling these errors when tail and crosswinds were simulated. Also, speed reduction during climbout as a result of turning at bank angles of 25-30 degrees may pose a problem.

Results from all the missed approach cases indicate lateral tracking error to be less than 20 feet for both front and back azimuth coverage. Vertical tracking errors during the descent part of the missed approach are well within acceptable limits. No problems were encountered when simulating a switch in guidance implementation involving altitude. During descent, the vertical guidance algorithm used the MLS-derived altitude. Capturing a barometric altitude, and switching the guidance algorithm to track this constant altitude, occurred without transients or disruption in operation.

RECOMMENDATIONS

Several areas of continued analysis and simulation have been identified as a direct result of the present study. Additional follow-on tasks are recommended that relate to different aspects of MLS operations other than departures and missed approaches.

The tasks recommended as a result of this study are:

- Investigate the problems with large bank angles during departures, especially with winds.

- Provide for speed control during the precision departures with turns.

- Formulate and analyze other situations involving the switch from MLS altitude to barometric altitude.

- Establish if there is an optimum time to switch from front azimuth coverage to back azimuth, and evaluate performance under these conditions.

- Investigate any problems encountered when leaving back azimuth coverage and entering en-route navigation.

- Develop algorithms that can cope with leaving back azimuth guidance then re-entering front azimuth coverage during a go around.

Additional follow-on tasks include:

- Simulating the conical azimuth and elevation angle scan geometry of the MLS with the elevation antenna offset laterally from the runway centerline.

- Evaluating the tracking performance when enroute navigation errors cause initial lateral and vertical offsets at entry to MLS coverage.

- Investigating changes to the guidance algorithms when the aircraft is ordered to change to another path while making an approach.

- Evaluating the lateral and vertical guidance laws using a fixed-base simulator with a pilot in the loop.

MLS OPERATIONS

Different modes of operation of the MLS are employed for departure guidance and for the missed approach guidance. For departure, precision distance measuring equipment (DME/P) is employed for range information, and a back azimuth (BAZ) transmitter provides the azimuth angular information. Figure 1 is a sketch of the departure geometry assumed for the present study. For missed approaches, the same DME/P is used with a front azimuth (AZ) transmitter and an elevation (EL) transmitter. Figure 2 shows this geometry. When the aircraft crosses the y-axis, the front azimuth mode is switched to the back azimuth mode. It is noted that back azimuth operation does not have elevation information available. Consequently, for purposes of the present study, it was assumed that altitude would be available to the MLS guidance computer. In this way, the coordinates of the aircraft can be uniquely determined for back azimuth operation. The following sections describe the calculations required to determine the aircraft position for both front and back azimuth modes of operation as a function of the angular and range information.

PRECISION DEPARTURE GEOMETRY

Position coordinates $(X'_m,\ Y'_m,\ Z'_m)$ of the aircraft MLS antenna may be calculated from the range, back azimuth angle, and the altitude. The expressions for those coordinates have been derived using the assumed geometry of Figure 1. Although straightforward, these calculations are somewhat complicated because the x-coordinate requires the solution to a quadratic equation. This fact necessitates logic to determine the sign on the radical in the equation for Xm' to assure the correct solution. In the following equations, the altitude h is assumed available from a source external to the MLS. The values of the distance X_B and X_D represent the transmitter locations at the 12000 foot runway at San Francisco.

$$z'_m = -h \tag{1}$$

$$x'_m = -\frac{b}{2} \pm \sqrt{\left(\frac{b}{2}\right)^2 - c} \tag{2}$$

$$y'_m = -\left[z'^2_m + (x'_m - x_B)^2\right]^{1/2} \tan \theta_{BAZ} \tag{3}$$

where:

$$b = -2\left[x_B + \cos^2\theta_{BAZ}(x_D - x_B)\right]$$

$$c = \left(x_B^2 + z_m^2\right) + \cos^2\theta_{BAZ}\left(x_D^2 - x_B^2 - R_{DME}^2\right)$$

$$x_B = -1700 \text{ FT}$$

$$x_D = 12000 \text{ FT}$$

Steps in the development of the above equations are given in Appendix A.

The sign on the radical in Equation (2) depends on the position of the aircraft relative to the DME transmitter. This sign reverses when the quantity under the radical passes through zero. Logic in the guidance computer is used to set and change this sign automatically. In the simulation, the position coordinates of the aircraft CG (X_m, Y_m, Z_m) are computed to account for the offset of the aircraft MLS antenna from the CG.

MISSED APPROACH GEOMETRY

For missed approaches, the position coordinates are computed from the azimuth angle, elevation angle, and DME range when the aircraft is in the front azimuth sector. As the aircraft passes to the back azimuth coverage, switching to the departure guidance equations occurs. Figure 2 shows the missed approach geometry from which the following equations have been derived:

$$y'_m = -R_{DME} \sin \theta_{AZ} \tag{4}$$

$$x'_m = x_D \cos^2\theta_{EL} - \left[\cos^2\theta_{EL}\left(R^2_{DME} - x^2_D \sin^2\theta_{EL}\right) - y'^2_m\right]^{1/2} \tag{5}$$

$$z'_m = -\left(x'^2_m + y'^2_m\right)^{1/2} \tan \theta_{EL} \tag{6}$$

The distance, R_{DME}, is obtained in both precision departures and missed approaches from the same transmitter, which is collocated with the front azimuth transmitter. The above equations are valid for the elevation antenna located on the runway centerline as shown in Figure 2. Actually, this antenna will be displaced laterally, which will result in somewhat more complicated equations. The effect of such a geometry on tracking performance is slight as compared to the results obtained in this study.

PRECISION DEPARTURE PATH DESCRIPTION

A specific airport and departure procedure was chosen to illustrate the performance of a precision departure using the MLS. San Francisco runway 28R was selected and a noise abatement takeoff procedure was employed. This procedure requires a sharp right turn just after takeoff to avoid terrain. Then, a path is flown over a sparsely populated area until over-water flight is attained.

DEPARTURE PATHS

Waypoints were defined that resulted in lateral paths suitable for MLS implementation. Three straight legs and two turns were used in the departure. Figure 3 depicts a typical ground track for this simulated MLS precision departure.

MLS vertical guidance was not used for this departure. Instead, two existing MD-80 autopilot modes, takeoff and speed select, were employed. At takeoff, the pitch autopilot was set in take-off mode and the gear was down. At 100 feet altitude, the gear was retracted. After the first turn, the pitch autopilot was switched to speed select mode where a target speed of 250 KT was input. At 165 KT, the flaps were retracted, and at 197 KT the slats were retracted. A summary of events for this departure are given in Table 1.

When flown visually, this departure requires a right turn with a relatively large bank angle to be made as soon as feasible. This turn is to avoid some mountainous terrain near the airport. When flown using the MLS, the departure paths are prescribed circular arcs defined by the ground speed and turn radius. Four paths were simulated to compare tracking accuracy and speed variations during the turns. These paths resulted in nominal, no-wind bank angles of 15, 20, 25, and 30 degrees. Waypoint data for these four cases are shown in Table 2. Results for these cases, under various wind conditions, are discussed in detail in later sections.

LATERAL GUIDANCE CONCEPTS

Lateral guidance for precision departure, as well as for back azimuth coverage during missed approaches, is identical to the approach guidance as documented in Reference 2 (p. 6-12). The concept used is to generate a steering signal that is input to the roll autopilot inner loop. During turns, this signal is based on the nominal bank angle (for a given turn radius and ground speed) and on error signals that are functions of lateral tracking error and error rate. During straight leg segments, the steering signal is only a function of lateral tracking error and error rate.

The only difference in departure operation lies in the way in which the waypoints are defined. For example, Figure 3 shows WP6 to be at the origin, and WP1 is arbitrarily selected along the desired radial. In this way, the roll steering commands can be computed in the same manner as for approaches simulated in previous studies (Reference 2).

MISSED APPROACH PATH DESCRIPTION

The same runway at San Francisco used for departures was also used for the missed approach cases. Two types of missed approaches were simulated. Both types used MLS lateral guidance throughout, switching to back azimuth when appropriate. Vertical MLS guidance was used prior to go around initiation, then MD-80 pitch autopilot modes were selected as appropriate.

APPROACH PATH

In the first set of cases, the aircraft was descending under lateral and vertical MLS guidance. At a specified altitude, a missed approach was initiated. At that time, the pitch autopilot was set in go-around mode whereas lateral MLS guidance was maintained. This procedure allowed study of lateral tracking accuracy during go around in the presence of noise and winds. Figure 4 is a sketch of the vertical profile for this set of cases.

In the second set of cases, pitch up to level flight was initiated at a specified altitude. Lateral and vertical guidance during this time was under MLS control. At a specified distance from the runway, go-around mode was initiated in the pitch autopilot (Figure 5). Lateral guidance, using the front azimuth coordinates (Equations (1) - (3)), was maintained until passing into the back azimuth sector. At that time, lateral guidance was switched and the back azimuth coordinates were used (Equations (4) - (6)).

LATERAL AND VERTICAL GUIDANCE CONCEPTS

No changes to the vertical guidance law (as described in Reference 2, p. 13, 14) were necessary for use in the missed approach studies. The lateral guidance law also was usable without change. Additional switching logic was required to change from front azimuth coordinates to back azimuth coordinates. This switching was programmed to occur at the y-axis crossover, when the X coordinate changed sign. It is noted that the runway is in both front and back azimuth coverage, so switching could occur anywhere in this region. For the present study, switching was chosen to be at the y axis for convenience.

SIMULATION RESULTS

SIMULATION DESCRIPTION

The basic simulation used for these studies is the same MD-80 program as used in previous studies (Reference 1 and 2) with only minor modifications for the missed approach cases. The existing MD-80 program was developed for landing only, and did not have the capability for takeoff when the aircraft was on the ground. Consequently, for precision departures, the aircraft was started at a low altitude and takeoff continued from that point.

Lateral and vertical steering signals were generated and input to the appropriate autopilot inner loops. No changes to these inner loops were made in the simulation. All required calculations, and the waypoint data storage, were external to the autopilot.

Wind and Turbulence Models

Winds (simulated as a function of altitude) and turbulence were used in the simulation. These models are the same as those used in the previous MLS landing studies Appendix B contains the details of these models, (Reference 2).

MLS Noise Models

Noise levels used in the departure and missed approach simulations are based on the models given in Reference 2. Appendix C shows these models for elevation and azimuth angles, and for DME range. All cases simulated for this study contained this MLS noise.

DEPARTURE CASES

Seven departure cases have been simulated using the San Francisco airport runway 28R. In order to realize the noise abatement benefits of this departure, the first turn must be executed as soon as feasible after takeoff and be tight enough to avoid nearby terrain. Results of four cases under different wind conditions compare path tracking accuracy. Three additional cases for different departure paths under the same wind environment were also simulated. Table 3 defines the bank angle and wind conditions for these seven cases. The second turn, after a short straight leg, is not critical and was selected to be nominally 15 degrees for all cases.

Case 1 - Path 1, No Wind

Shown in Figure 6 is the bank angle time history for Path 1 (a 20 degree nominal bank turn). Some overshoot is experienced in the no-wind case and is due to the tracking error inherent in the aircraft roll response. At the end of the first turn, the bank angle tends to zero for the short straight leg. Then, the 15 degree bank turn is executed to place the aircraft along the desired radial.

At the end of the first turn (about 70 seconds), the pitch autopilot is switched to a speed command mode, where 250 knots is set as the target speed. Flaps and slats are retracted as given in the schedule of Table 2. The resulting speed profile is shown in Figure 7. During the first turn, the speed varies about 2 to 3 knots from the desired 158 KT, then increases up to the 250 KT target speed. This run was terminated arbitrarily at 150 seconds, which was before the speed had reached steady state.

During this entire time, MLS lateral guidance was employed to keep the aircraft on the desired lateral path. Figure 8 shows this lateral tracking error, both for the turns and for the straight legs. At the transition to the straight portion (at about 22 and 36 seconds), there is an abrupt change in the error. This change is due to switching guidance laws from a circular track to a linear track.

This tracking error can be expressed in terms of dots in a similar manner to landing approaches. Figure 9 is the assumed lateral tracking error sensitivity definition. The envelope shown defines the ± 2 dot boundary. It is defined as a function of along-track distance (i.e., the actual curved path the aircraft is flying) as opposed to the straight extended runway centerline as used for present ILS approaches. Figure 10 shows the tracking error as a function of along-track distance for a full scale of ± 2 dots. At the end of the runway, 2 dots represents 350 feet. The sensitivity varies linearily along a 3 deg slope, until at about 33000 feet, 2 dots represents 1500 feet. At distances greater than this value, the sensitivity remains at 1500 feet. As can be seen from Figure 10, tracking for this case is within ± 1/4 dot during the entire departure.

Shown in Figure 11 is the resulting ground track for case 1. Back azimuth coverage is limited to ± 40° from antenna boresight. For the 28R departure, the back azimuth antenna will have to be skewed approximately 20° from the runway centerline to provide coverage for the second turn and straight leg.

Case 2 - Path 1 with Left Cross wind

In this case, a tail and cross wind were added as external disturbances (Table 3). The resulting bank angle is given in Figure 12. Comparing this response to the no-wind case of Figure 6, one sees the increased bank angle response due to the wind components. As the aircraft turns in this wind, the bank angle varies accordingly. The second turn is now at a bank angle of about 18° instead of 15°. A larger speed variation occurs for this case as shown in Figure 13. A 6 knot decrease in speed occurs near the end of the first turn, then the speed increases due to the pitch autopilot switching to a speed hold mode. Lateral tracking errors are larger than the no-wind case. Figure 14 shows peak errors to be within ± 200 feet as compared to the somewhat smaller peaks for the no-wind case. This error tends to zero as the second straight leg is being tracked (at distances of 35000 feet and greater). Lateral tracking degradation can also be seen by comparing the error in dots of Figure 15 with Figure 10. This particular wind condition produces tracking errors on the order of ± 1/2 dot.

Case 3 - Path 1 with Wind and Turbulence

Turbulence, as defined in Appendix B, was added to the steady portion of the tail and cross winds for this path. Comparing the bank angle, velocity, and tracking error, Figures 16-19 (Case 3), with Figures 12-15 (Case 2) shows only a slight increase in activity due to the turbulence. Since a statistical analysis was not performed due to time constraints, this is the only case in which turbulence was simulated. It was included to give a general idea of response in a turbulent environment.

Case 4 - Path 1 with Right Crosswind.

In this case, the direction of the cross wind is reversed from the wind in the previous cases, but has the same tail wind. This opposite direction wind results in a smaller bank angle during the second part of the first turn (Figure 20).

The second bank angle is also smaller during the first part of the turn. Speed variation during the first turn (Figure 21) is somewhat less than Case 2 (Figure 13).

Tracking errors (Figures 22 and 23) are on the same order of magnitude as Case 2 with the left crosswind (Figure 14 and 15). However, the error at the end of the first turn for the left crosswind is about 150 feet to the left of desired track. This is a more critical case from terrain avoidance considerations. A right cross wind causes a 100 foot error to the right of desired track at the end of the first turn. The left cross wind will be simulated as being the more critical direction in the remaining cases where other paths are flown.

Cases 5, 6, and 7 - Paths 2, 3 and 4

These three cases are included so a comparison of performance can be made when other bank angles are employed for the first turn. The bank angle for Path 2 (a 15 degree nominal bank) in Figure 24A appears reasonable in the wind environment, but Paths 3 and 4 (25 and 30 degree nominal banks), Figures 24 B and C, show bank angle responses that are a result of exceeding existing command limits in the autopilot. Consequently, non-linear operation causes large tracking errors for these two cases (Figure 25 B and C). Even though visual departure at 28 R are flown at these bank angles, use of the autopilot would cause excessive errors. It is not considered likely that these large angles could be implemented without changing the autopilot inner loop limits and possibly some gains. No attempt to make such changes was considered in the present study. It is noted that results shown for Path 4 did not have the tail or crosswinds present. This wind case was simulated, but the wind levels were such that the autopilot saturated due to its internal bank command limits. Such a turn would not be possible with these assumed winds. Further study of gain and/or limit changes in the autopilot for this case is indicated.

A sketch of the ground tracks during the first turn for the four paths is shown in Figure 26. This figure, which is approximately to scale, shows Path 2 passing over the mountainous terrain. The simulation results for this case give the altitude near the end of the first turn to be 2800 feet. It appears that Path 1 would result in a departure that avoids the terrain problem with reasonable tracking errors.

MISSED APPROACH CASES

Six cases were simulated at San Francisco 28R for missed approach conditions (Table 4). Guidance for these cases used both front azimuth and back azimuth sectors and signal switching occurred between the coverages. In all cases, the aircraft was initially descending along a 3° glideslope.

The first three cases simulated a go around at 200 feet altitude. At that time, vertical guidance was switched from MLS control and the pitch autopilot was placed in the go around mode (see Figure 4). The desired lateral path was along the extended runway centerline and lateral guidance was under MLS control for the entire simulated missed approach.

The second three cases represent a change in the approach procedure as might be directed by air traffic control. Level flight is desired at an altitude of 1000 feet, so a pitch up is initiated at that time. This path is maintained until go around is directed at a specified distance from threshold (see Figure 5). Vertical MLS guidance is maintained until go around. MLS lateral guidance is used throughout, with switching to back azimuth coverage when the aircraft crosses the y axis.

In all cases simulated for these missed approaches, the bank angle error was less than 1°. Similarly, the lateral tracking error was always less than 10 feet. As a result, vertical tracking is of more interest, so the following discussions will focus on the vertical errors rather than on lateral performance.

Case 8 - No Wind

This case contains no external wind disturbances but does contain MLS angle and range noise. Go around is initiated at a time of 25 seconds, and the aircraft pitches up to a new attitude near 20° (Figure 27). The corresponding altitude changes are shown in Figure 28. This case, and subsequent cases, were simulated for an arbitrary 100 second period.

Vertical tracking error is computed and used by the MLS vertical guidance algorithm until go around is initiated. At that time, this error is no longer updated or used since the pitch autopilot is now in go around mode. Figure 29 is a plot of the vertical error as a function of time for this case. The corresponding error rate is shown in Figure 30. The dispersion in these plots is due to the MLS noise on the angle and range signals used by the guidance algorithm.

Tracking error and error rate may be plotted also as a function of distance to go. This distance is measured along the x axis to the aircraft, and is always considered positive. Figures 31 and 32 show the vertical errors as a function of the distance to go. For comparison purposes, the remaining missed approach cases will show the tracking error as a function of this distance.

Case 9 - Tail and Cross winds

Peak tracking errors for this case with winds increased by about a factor of 2 over Case 8, whereas the peak error rates remained about the same (Figures 33 and 34). This increase is not significant since the tracking errors remain small even in a wind environment.

Case 10 - Tail and Cross Winds with Turbulence

Addition of turbulence to the steady winds increased the peak tracking errors by another factor of 2, so now the peak is near 25 feet as compared to 14 feet for no turbulence and 6 feet with no wind at all. At go around initiation, the tracking error is about 23 feet (Figure 35).

Case 11 - Pitch Up - No Wind

This case represents a procedure as pictured in Figure 5 where pitch up from a 3° descent is made at 1000 feet altitude. Go around is initiated at a specified distance, and the pitch autopilot is engaged at that time. The resulting altitude is shown in Figure 36. Pitch attitude is given in Figure 37, and the vertical tracking error (during MLS guidance) is shown in Figure 38. At a distance to go of about 2000 feet, transition to level flight is made as marked by the abrupt change in tracking error. After capture, the error is within a few feet until the MLS mode is terminated and go around is initiated.

Case 12 - Pitch Up With Tail and Cross Winds

Vertical tracking error is somewhat increased for this case, but the altitude is nearly the same (Figure 39) in this simulated wind environment as compared to the no wind case shown in Figure 36 (Case 11).

Case 13 - Pitch Up Using Barometric Altitude

In this case, the MLS-computed altitude is used while descending along the 3° glideslope. At the time of pitch up, barometric altitude is used instead of the MLS altitude. The barometric altitude is used in both the switching logic to determine when the transition is made as well as during the altitude hold period.

Figure 40 is a plot of the resulting altitude for this case. There is little difference between this trace and the altitude resulting when no switching occurred (Figure 39). No problems were encountered in this case, and it appears switching to barometric altitude at some point in the approach can be made smoothly.

REFERENCES

1. J. B. Feather: Guidance Law Simulation Studies for Complex Approaches Using the Microwave Landing System (MLS), NASA CR-178182, November 1986.

2. J. B. Feather: Guidance Studies for Curved, Descending Approaches Using the Microwave Landing System (MLS), NASA CR-178030, May 1986.

TABLE 1

SEQUENCE OF EVENTS FOR DEPARTURE

1. Initial climb with pitch autopilot in takeoff mode.

2. Retract gear at 100 feet altitude.

3. Start right turn at end of runway to a 030° heading.

4. At end of turn, switch pitch autopilot to speed mode and select 250 KT speed.

5. Retract flaps at 165 KT, retract slats at 197 KT.

6. Make 15° left turn to intercept the radial R-342.

7. Return wings level and maintain desired course until end of simulated run.

TABLE 2

DEPARTURE WAYPOINT DATA

PATH NO.	NOMINAL, NO WIND BANK ANGLE (DEG)	WP1		WP2		WP3		WP4		WP5		WP6	
		X	Y	X	Y	X	Y	X	Y	X	Y	X	Y
1	20	26372.	40000.	16476.	22146.	15583.	11937.	16862.	8219.	11000.	0.	0.	0.
2	15	26372.	40000.	18897.	26514.	18004.	16303.	19310.	11930.	11000.	0.	0.	0.
3	25	26372.	40000.	15242.	19921.	14349.	9711.	15513.	6327.	11000.	0.	0.	0.
4	30	26372.	40000.	14506.	18592.	13612.	8382.	14708.	5158.	11000.	0.	0.	0.

TABLE 3

DEPARTURE CASES

CASE NUMBER	PATH NUMBER	TAIL WIND (KNOTS)	CROSS WIND (KNOTS)	TURBULENCE
1	1	NONE	NONE	NONE
2	1	10	15	NONE
3	1	10	15	YES
4	1	10	-15	NONE
5	2	10	15	NONE
6	3	10	15	NONE
7	4	NONE	NONE	NONE

TABLE 4

MISSED APPROACH CASES

CASE NUMBER	TAIL WIND (KNOTS)	CROSS WIND (KNOTS)	TURBULENCE	NOTES
8	NONE	NONE	NONE	GO AROUND AT 200' ALT
9	10	15	NONE	AT 200' ALT
10	10	15	YES	AT 200' ALT
11	NONE	NONE	NONE	PITCH UP
12	10	15	NONE	PITCH UP
13	10	15	NONE	PITCH UP (BARO ALT)

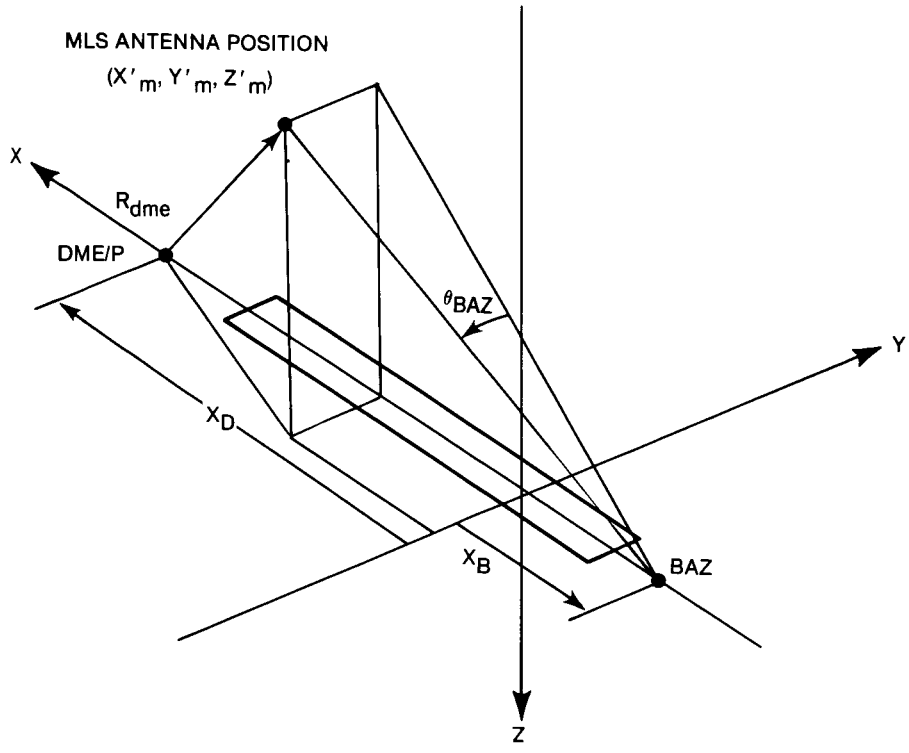

Figure 1. Departure Geometry

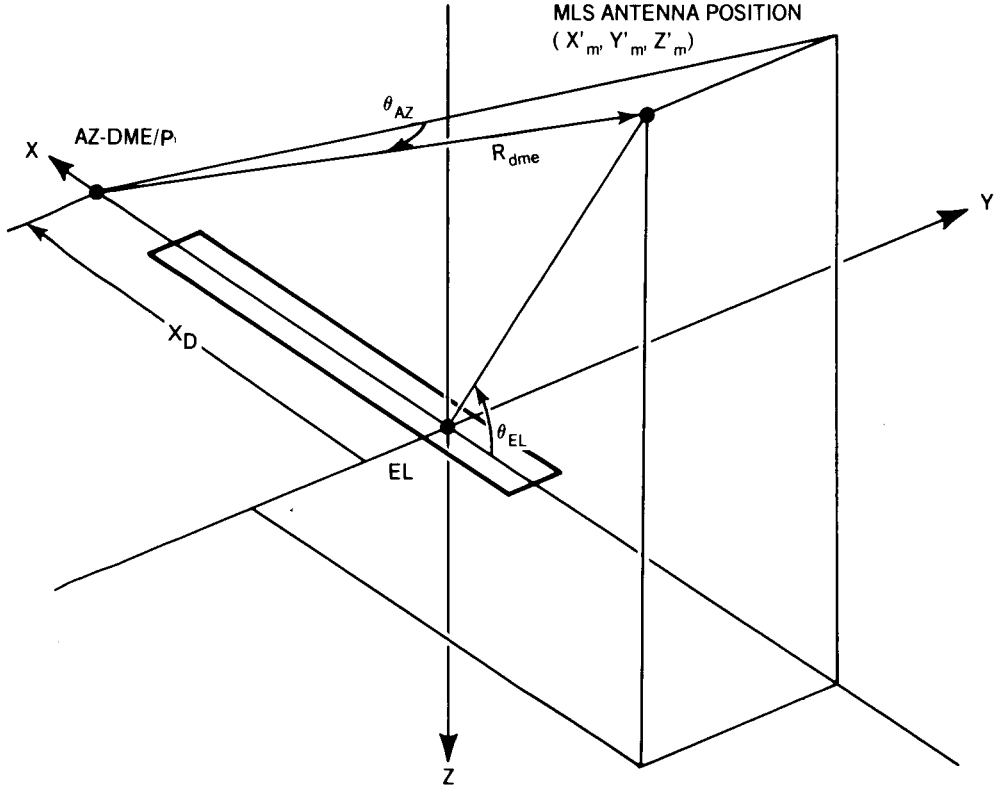

Figure 2. Missed Approach Geometry

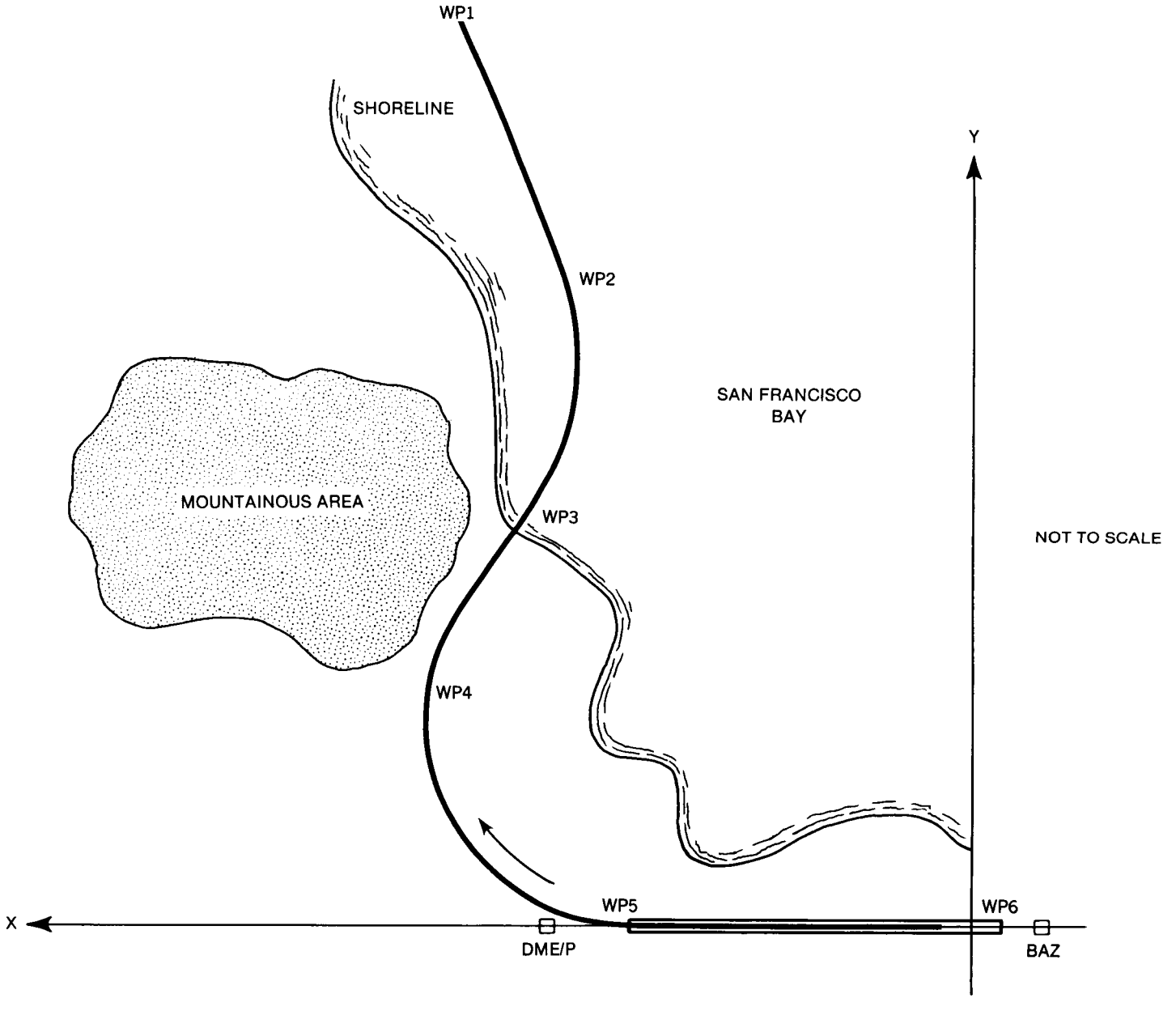

Figure 3. Typical Departure Path for San Francisco Runway 28R

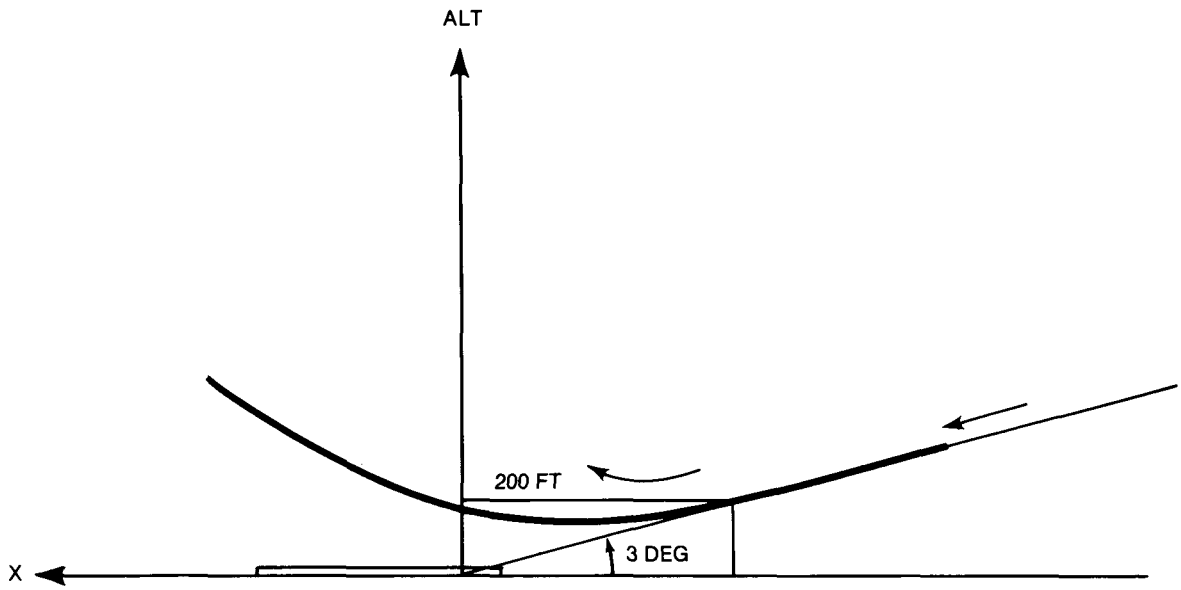

Figure 4. Typical Vertical Path for Missed Approach (Go-Around)

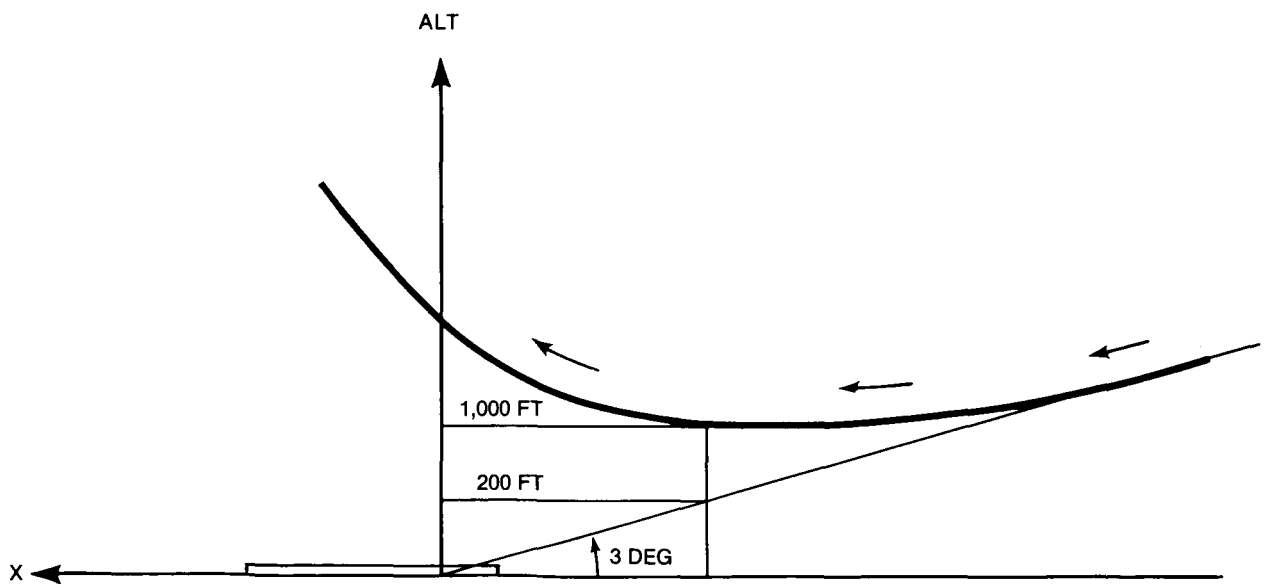

Figure 5. Typical Vertical Path for Missed Approach (Altitude Hold — Go-Around)

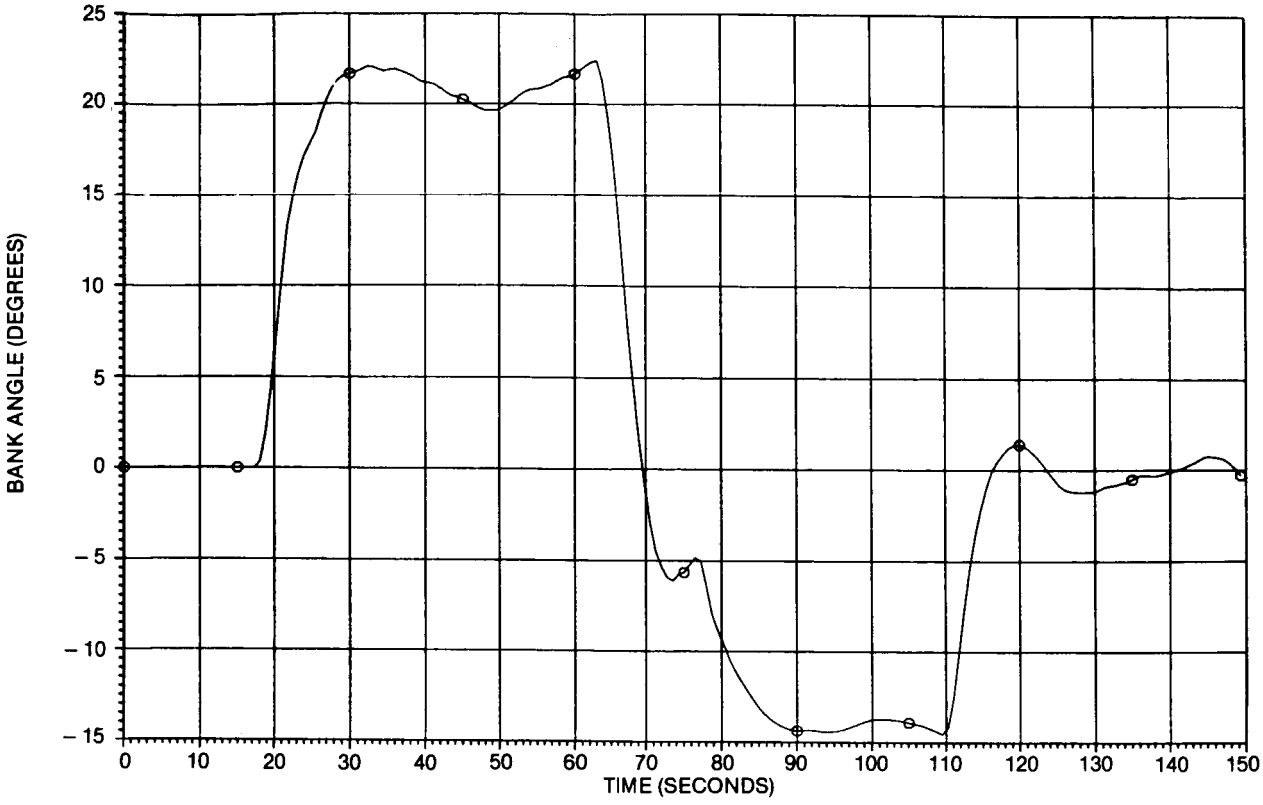

Figure 6. Bank Angle Time History for Path 1 (Case 1)

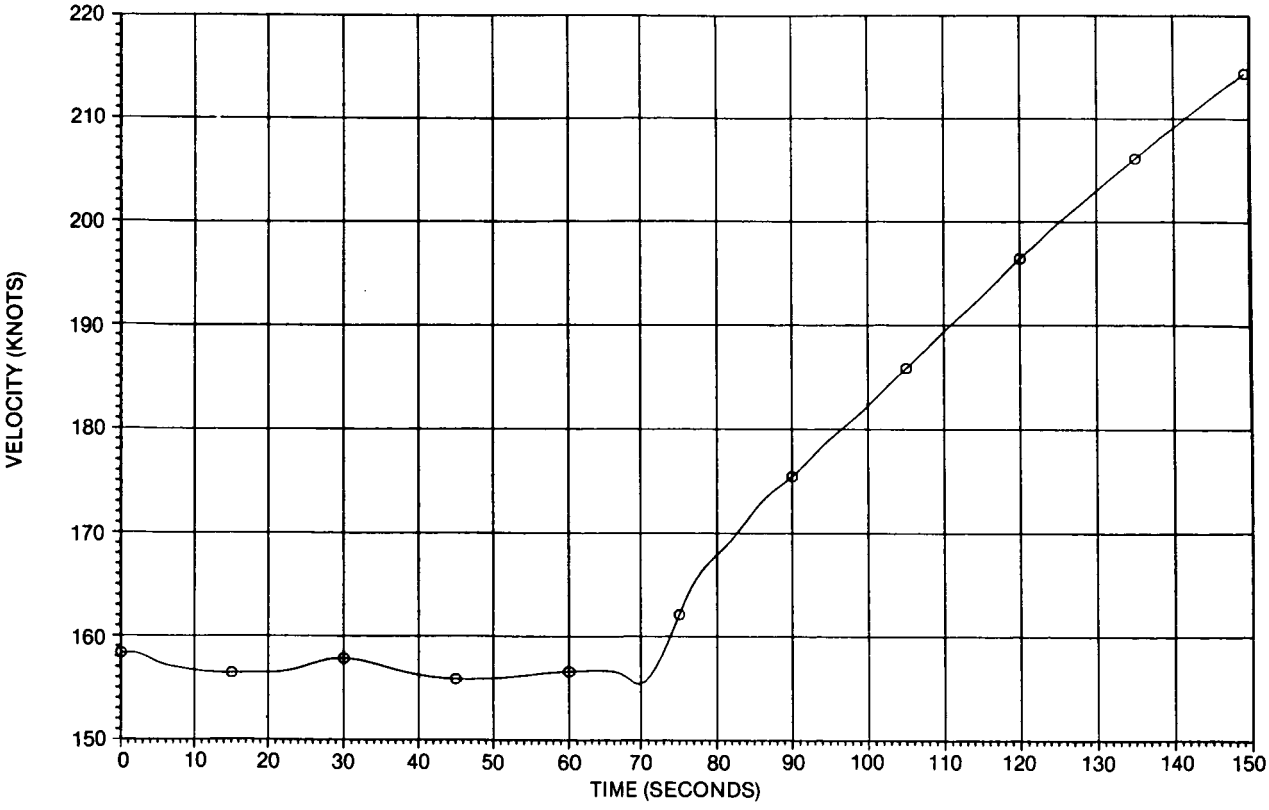

Figure 7. Velocity Time History for Path 1 (Case 1)

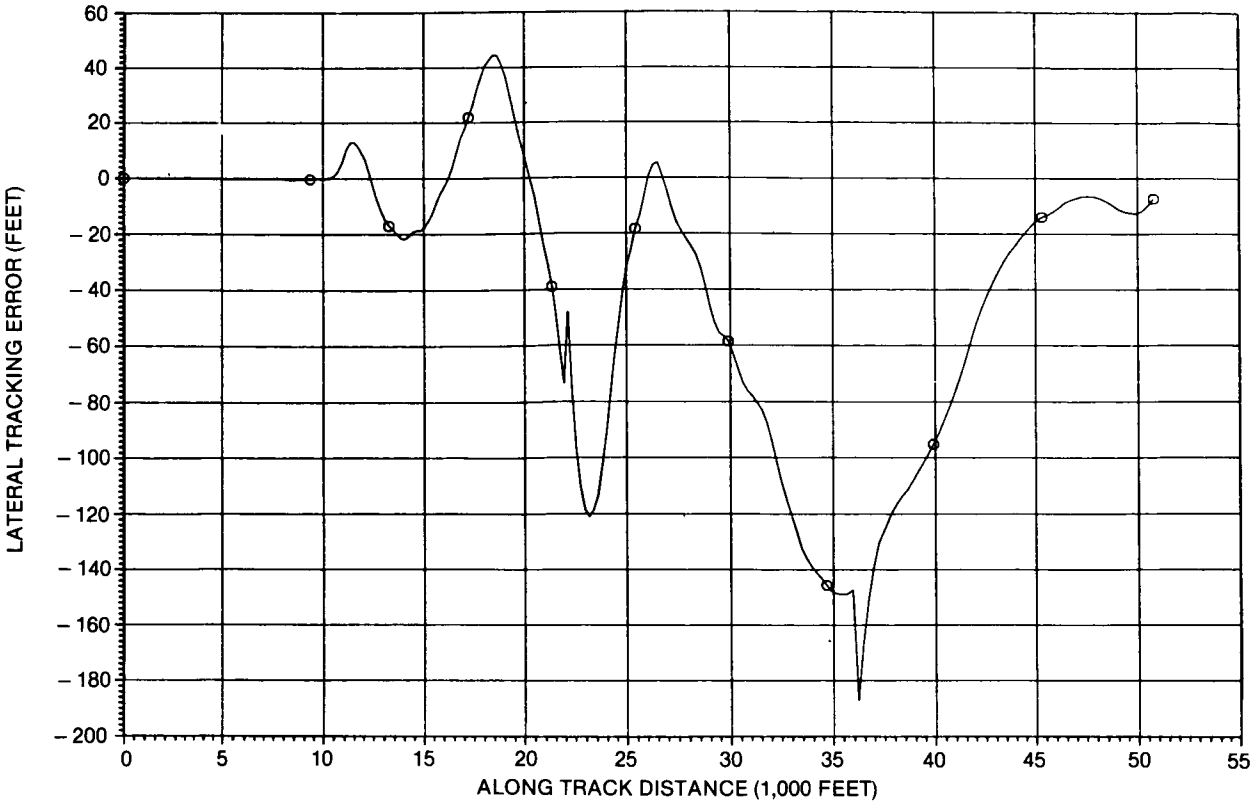

Figure 8. Lateral Tracking Error for Path 1 (Case 1)

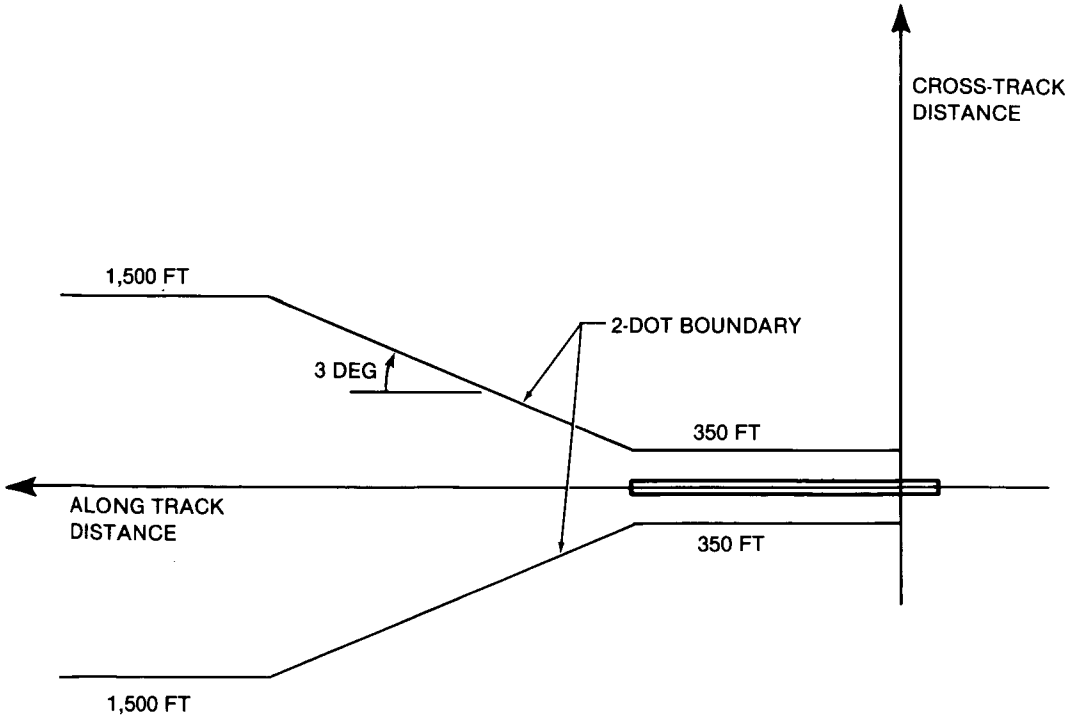

Figure 9. Lateral Tracking Error Sensitivity Assumed in Back Azimuth Coverage

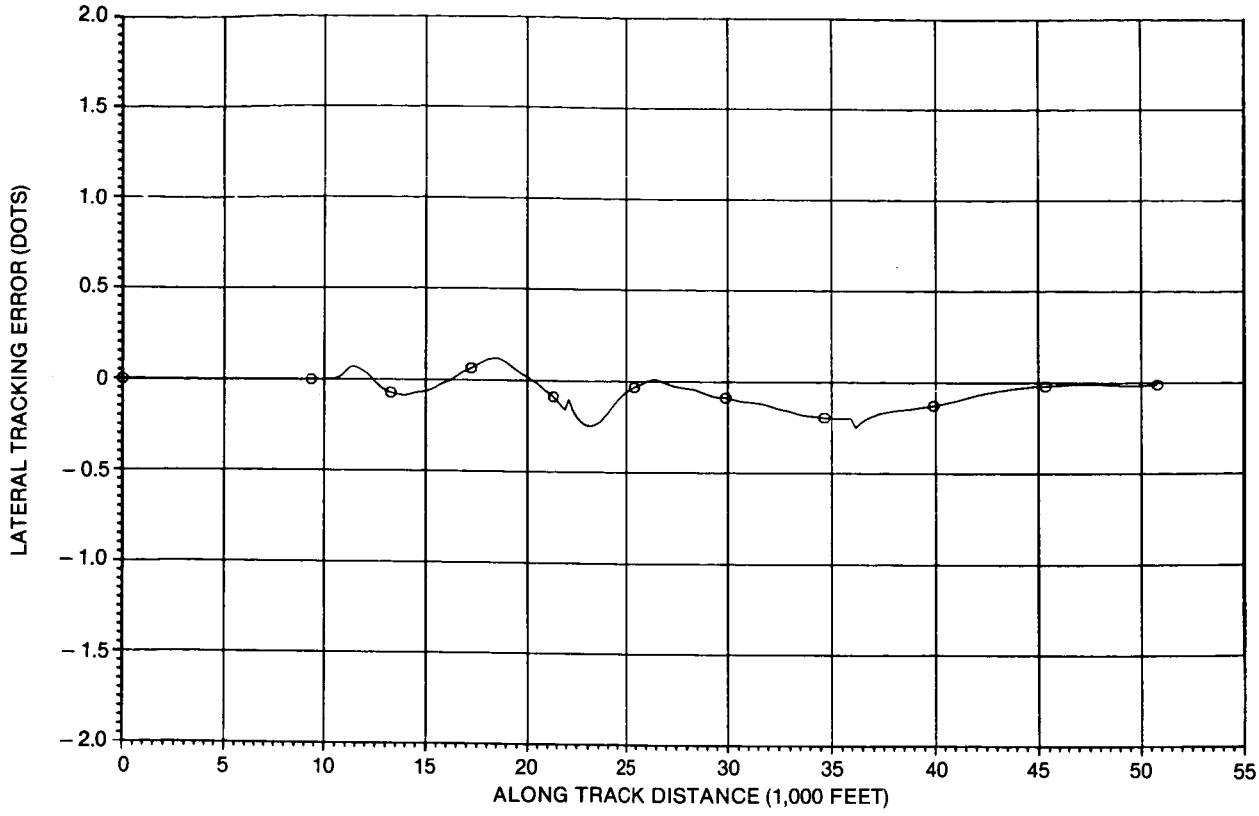

Figure 10. Lateral Tracking in Dots for Path 1 (Case 1)

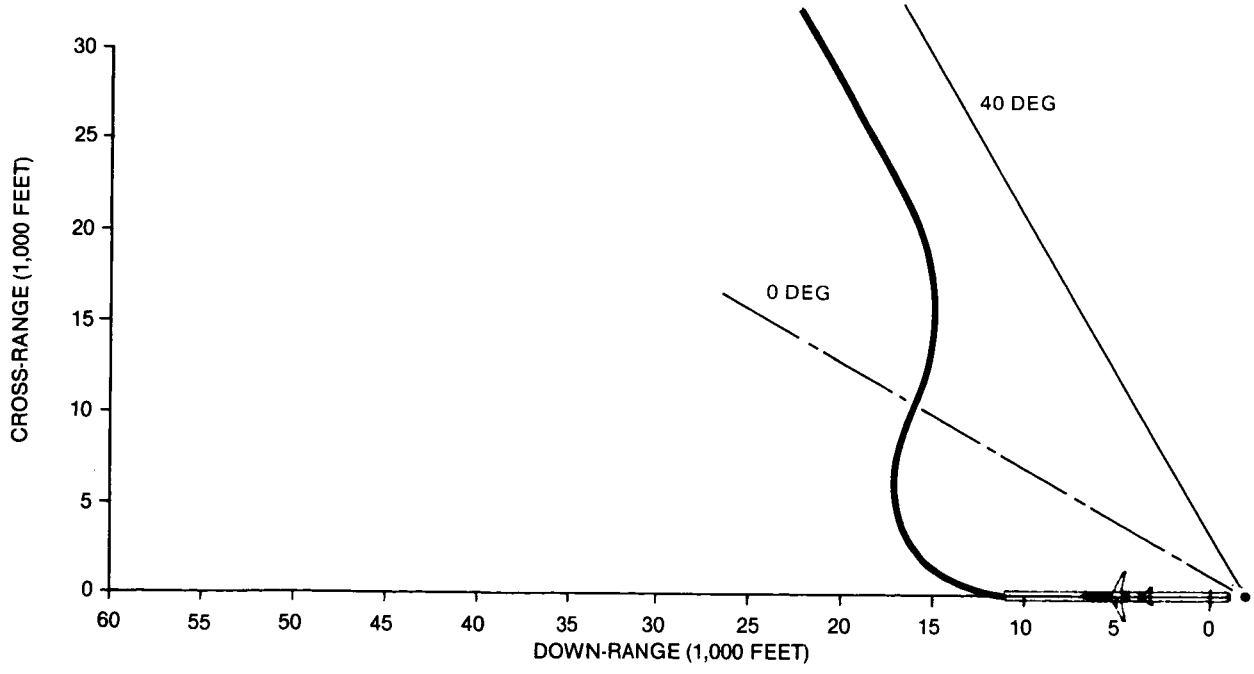

Figure 11. Ground Track for Path 1 (Case 1)

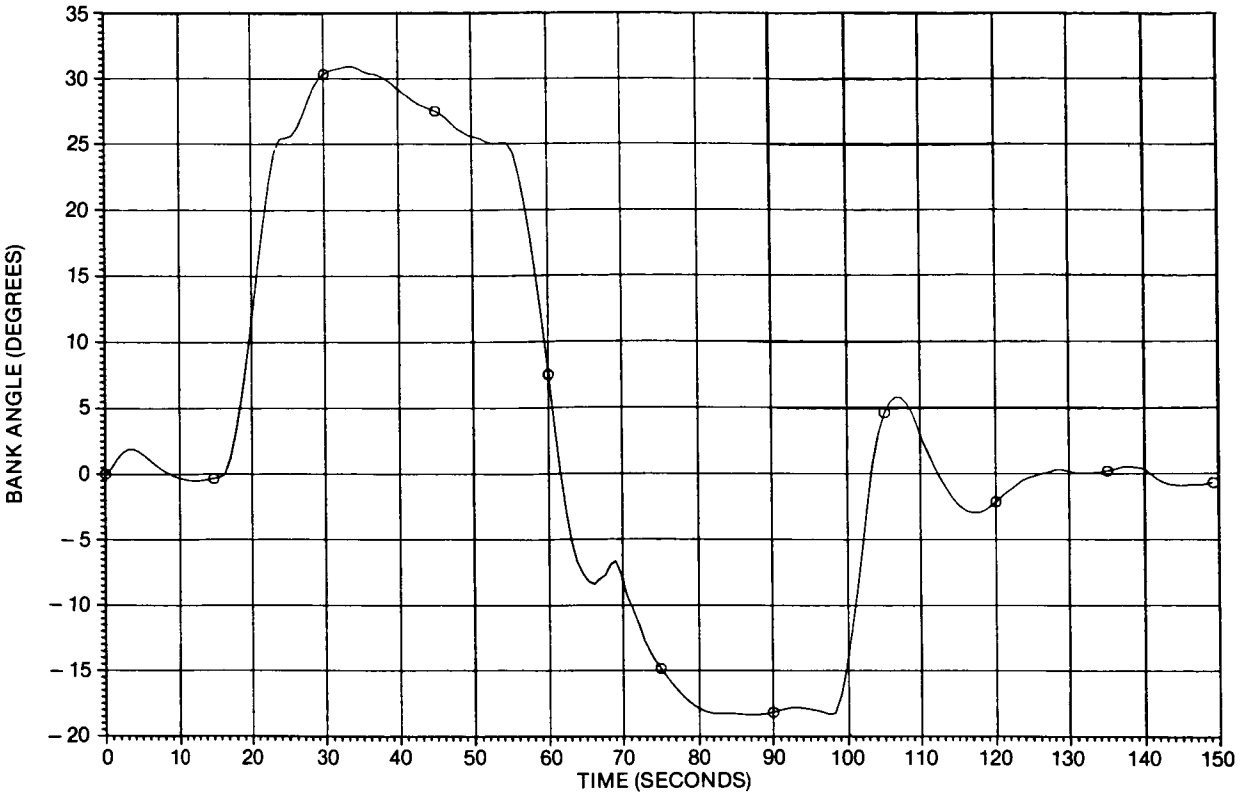

Figure 12. Bank-Angle Time History for Path 1 (Case 2)

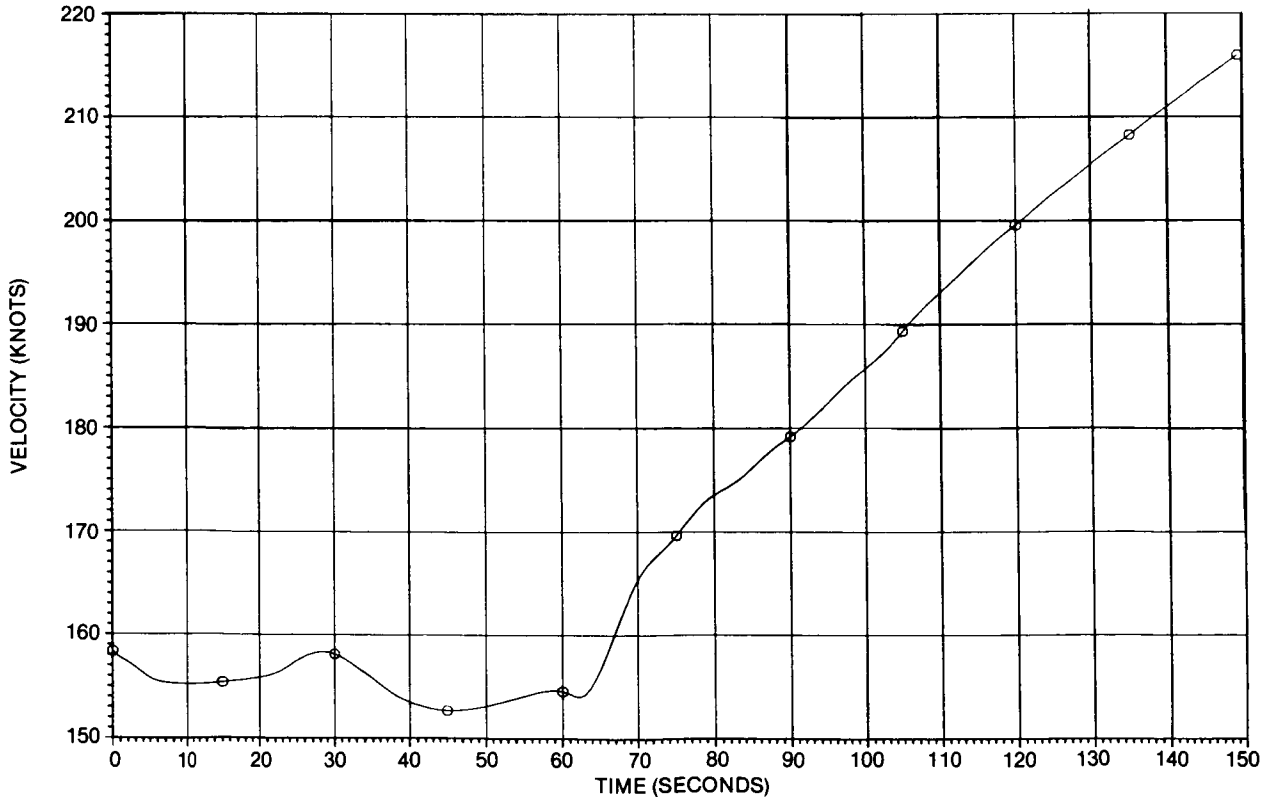

Figure 13. Velocity Time History for Path 1 (Case 2)

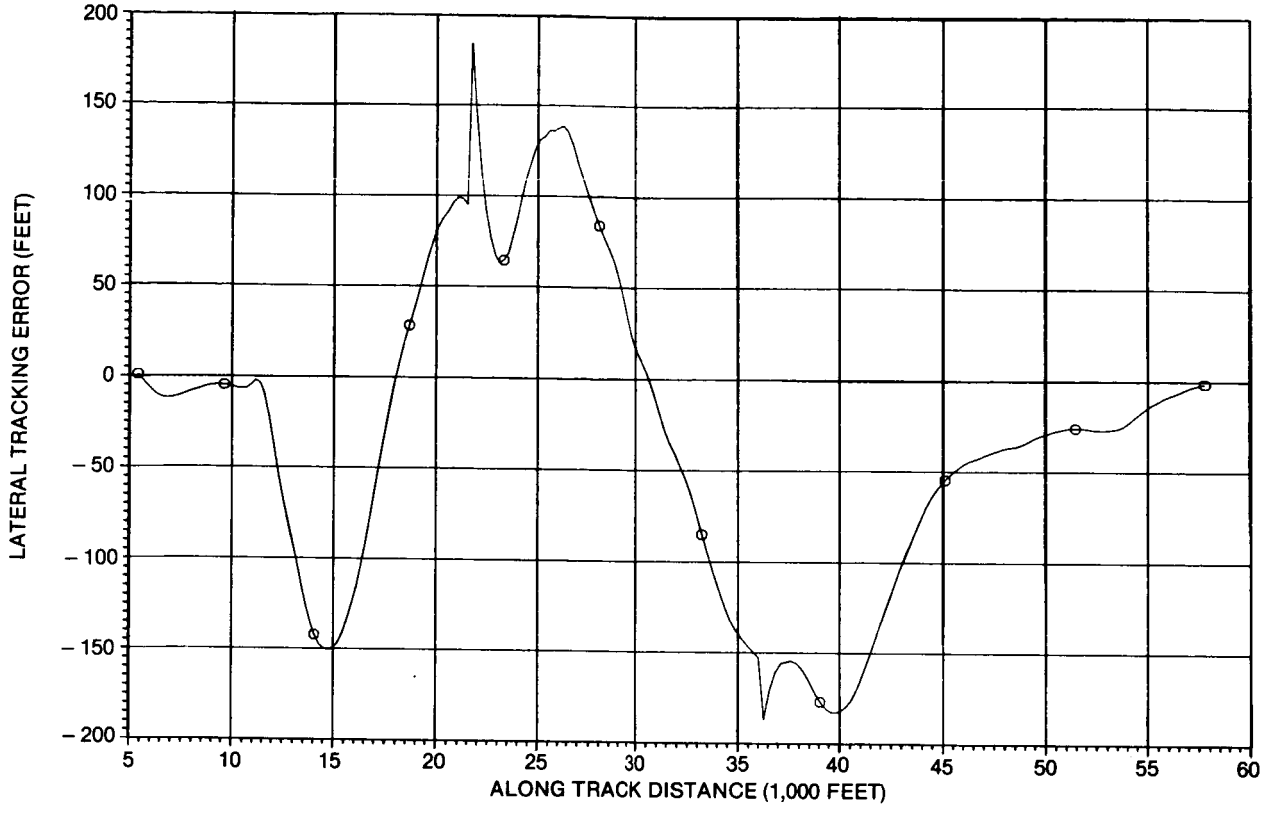

Figure 14. Lateral Tracking Error for Path 1 (Case 2)

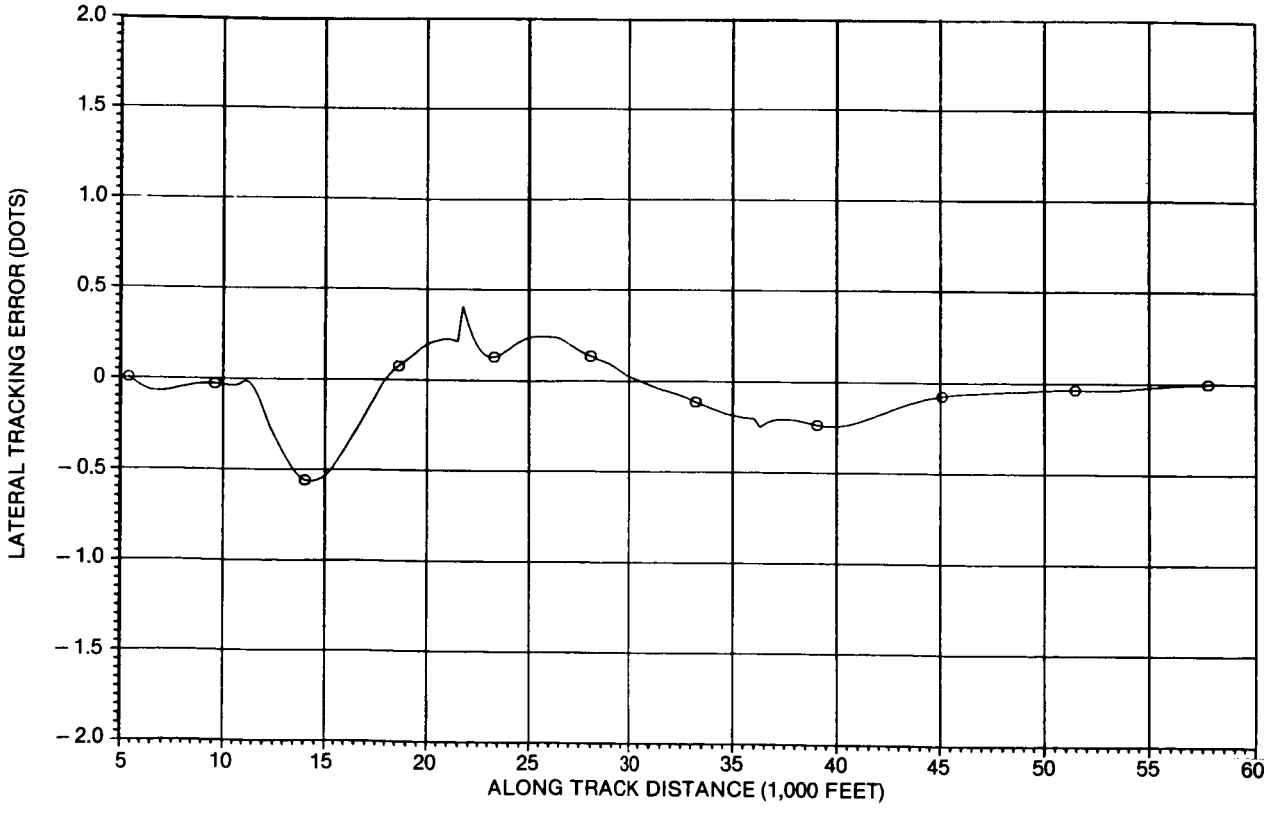

Figure 15. Lateral Tracking Error in Dots for Path 1 (Case 2)

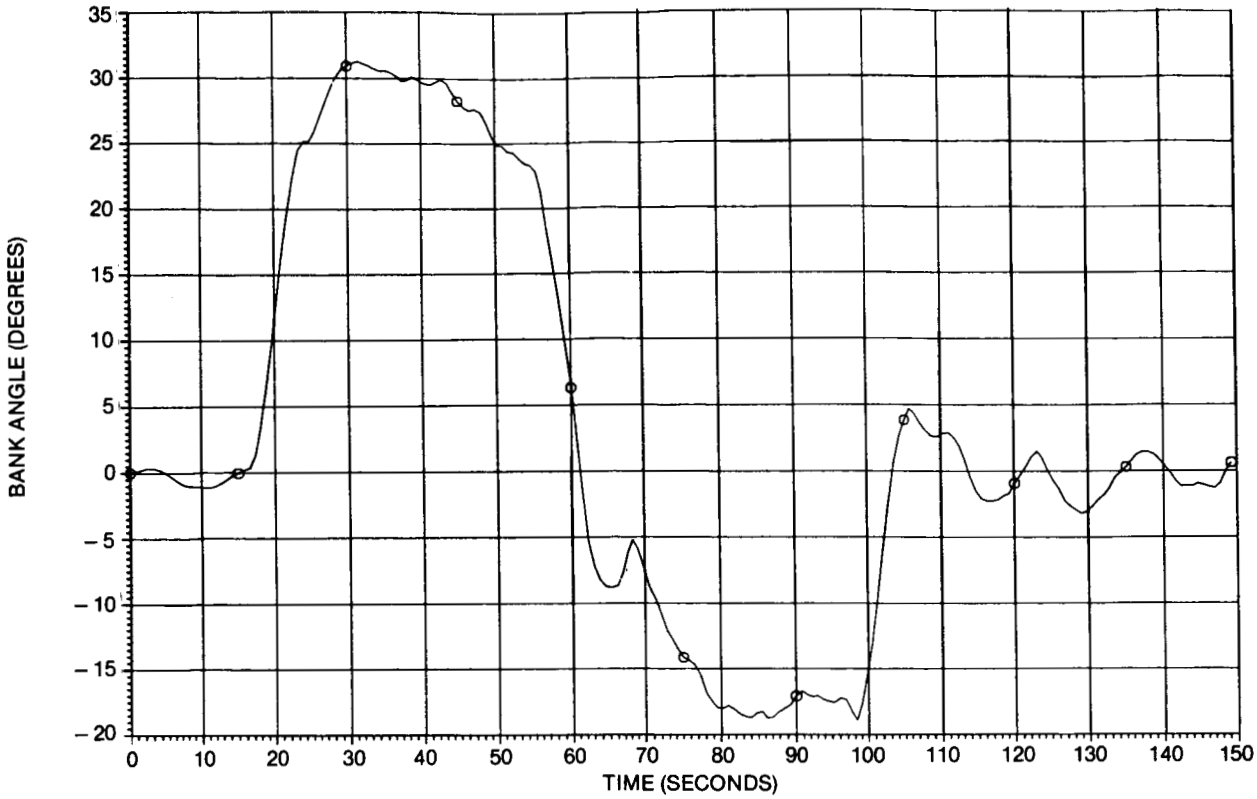

Figure 16. Bank-Angle Time History for Path 1 (Case 3)

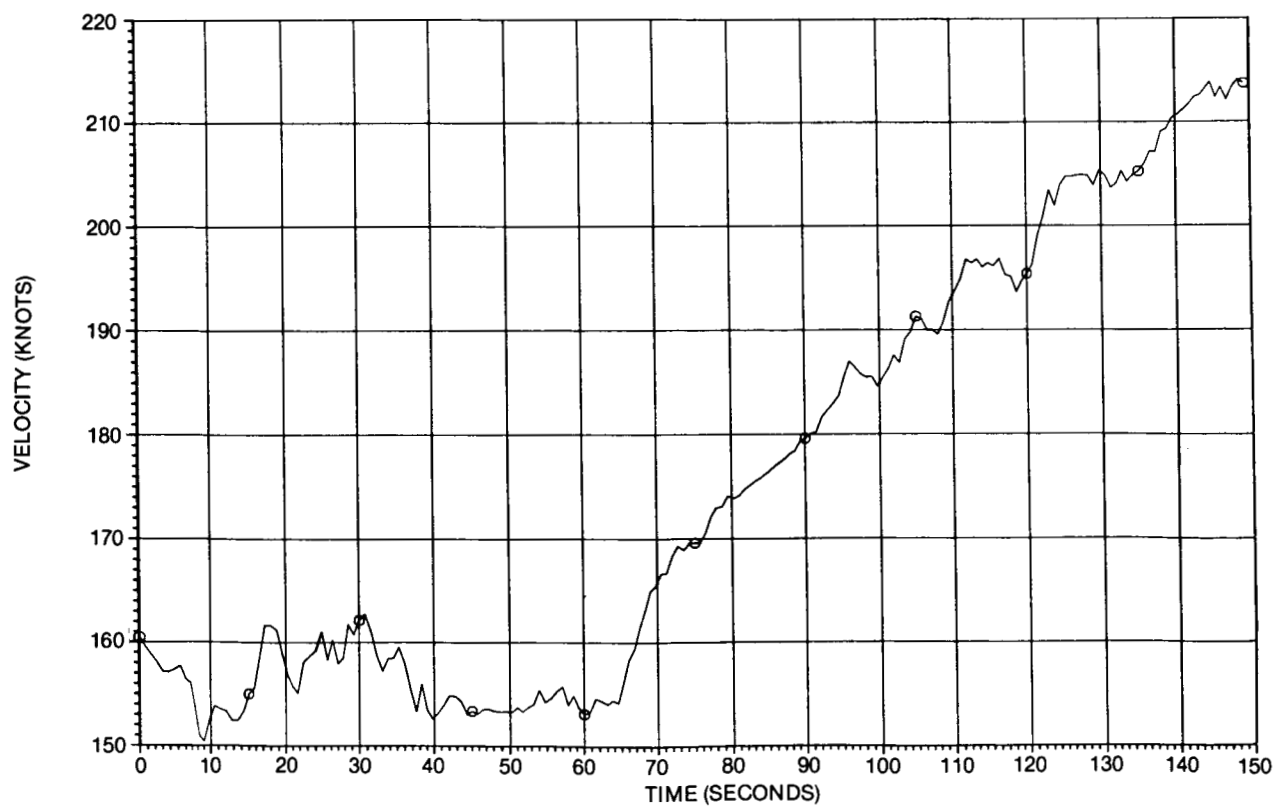

Figure 17. Velocity Time History for Path 1 (Case 3)

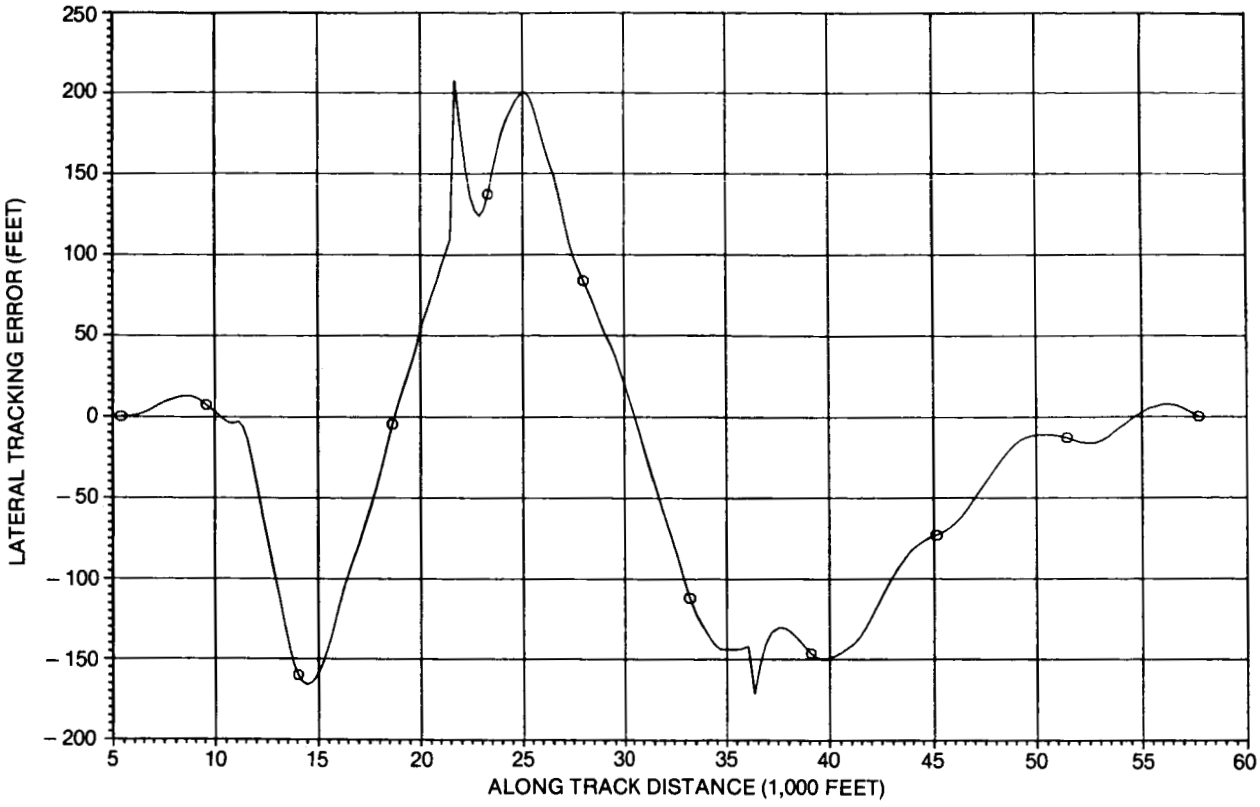

Figure 18. Lateral Tracking Error for Path 1 (Case 3)

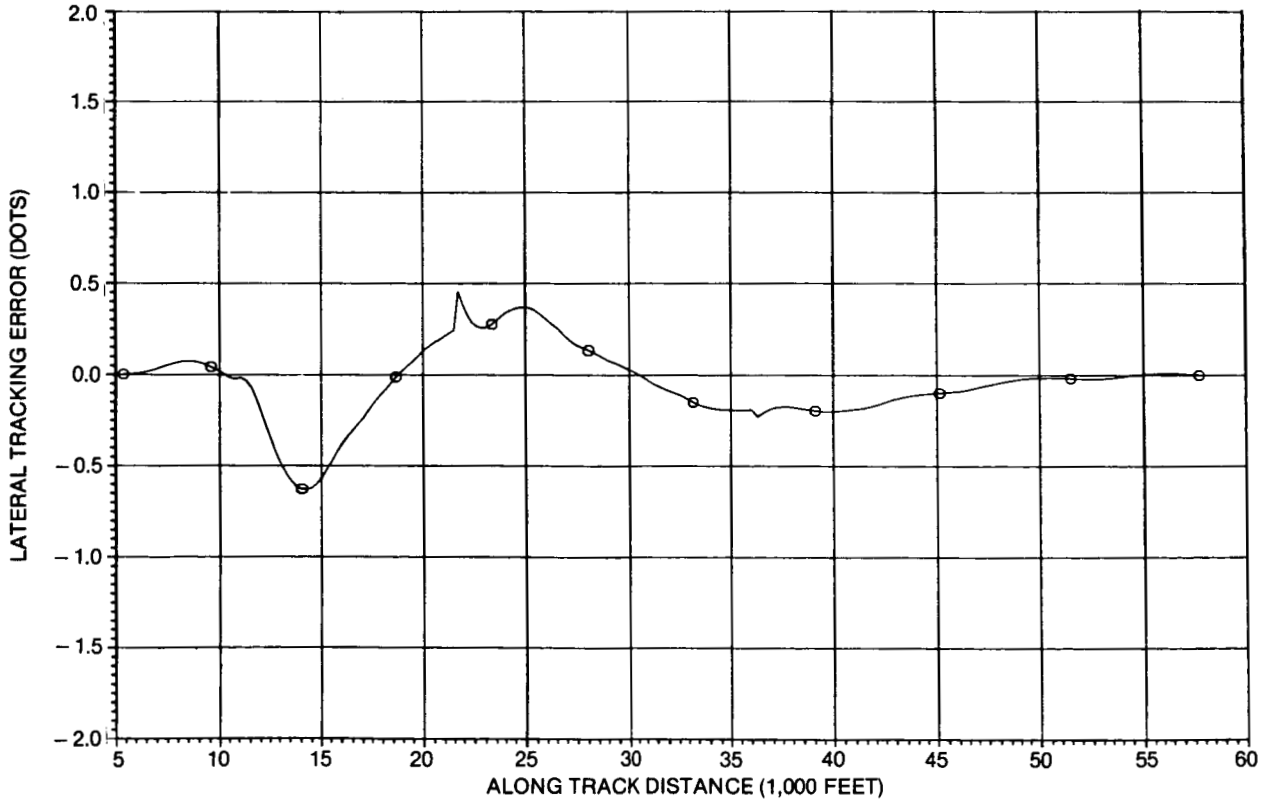

Figure 19. Lateral Tracking Error in Dots for Path 1 (Case 3)

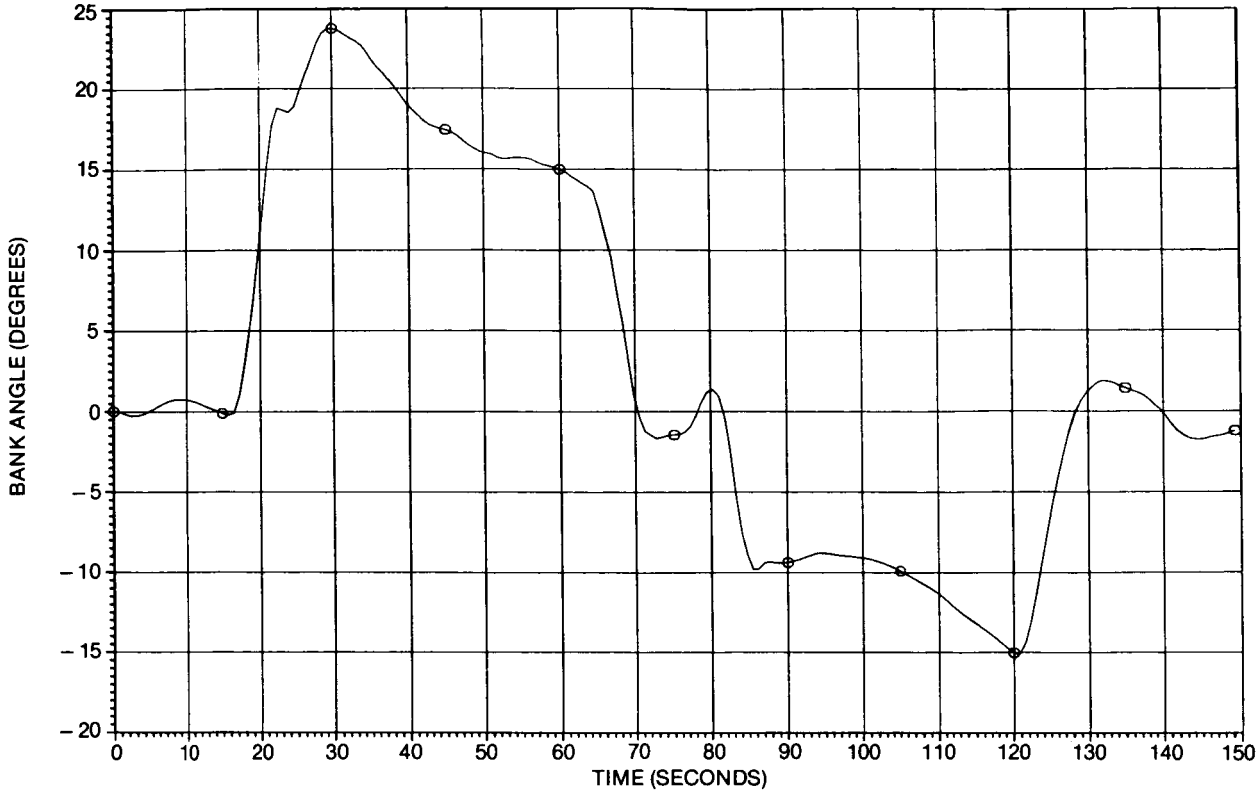

Figure 20. Bank-Angle Time History for Path 1 (Case 4)

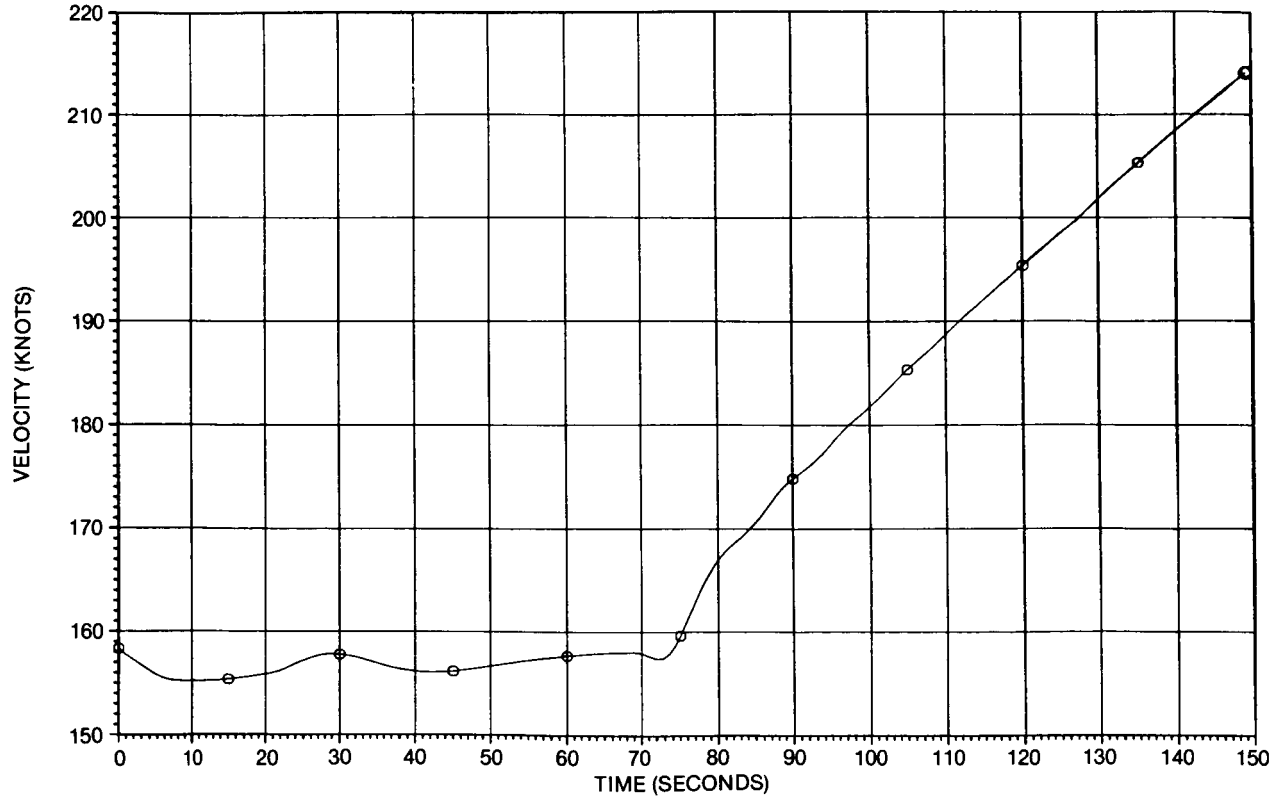

Figure 21. Velocity Time History for Path 1 (Case 4)

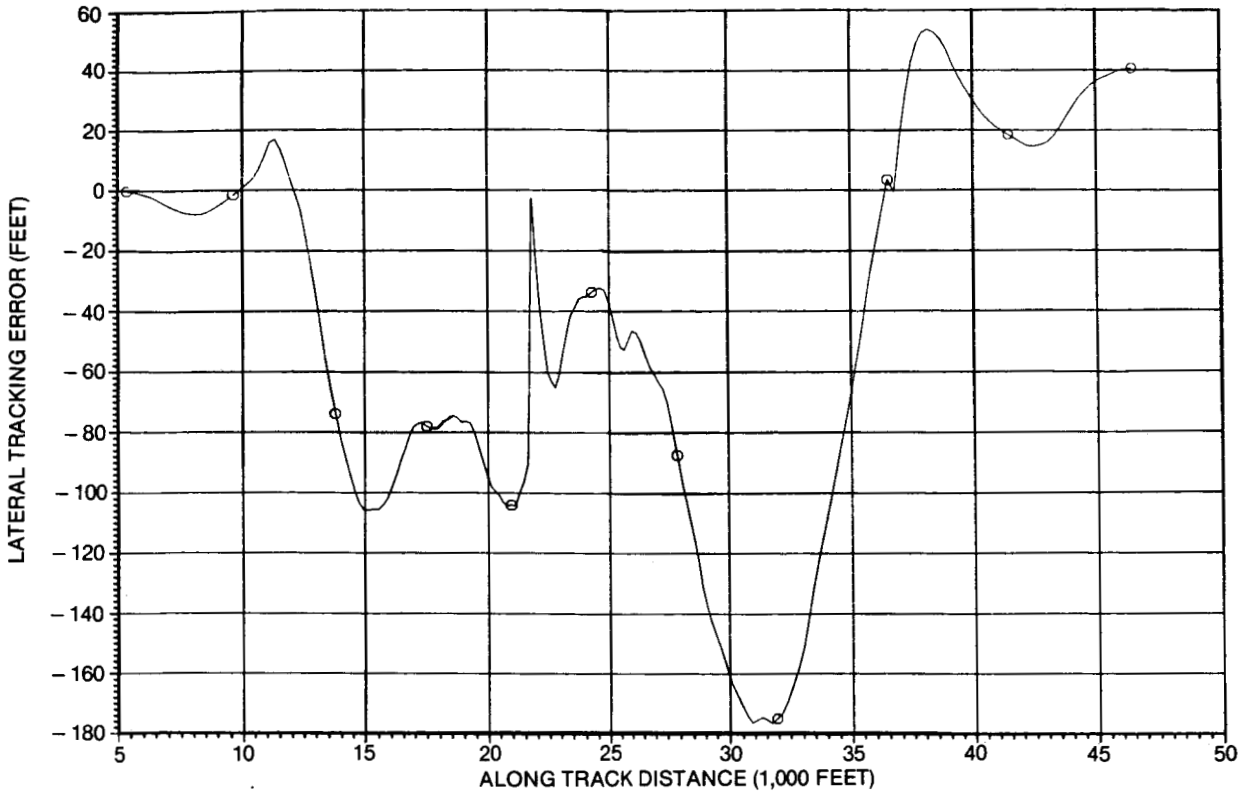

Figure 22. Lateral Tracking Error for Path 1 (Case 4)

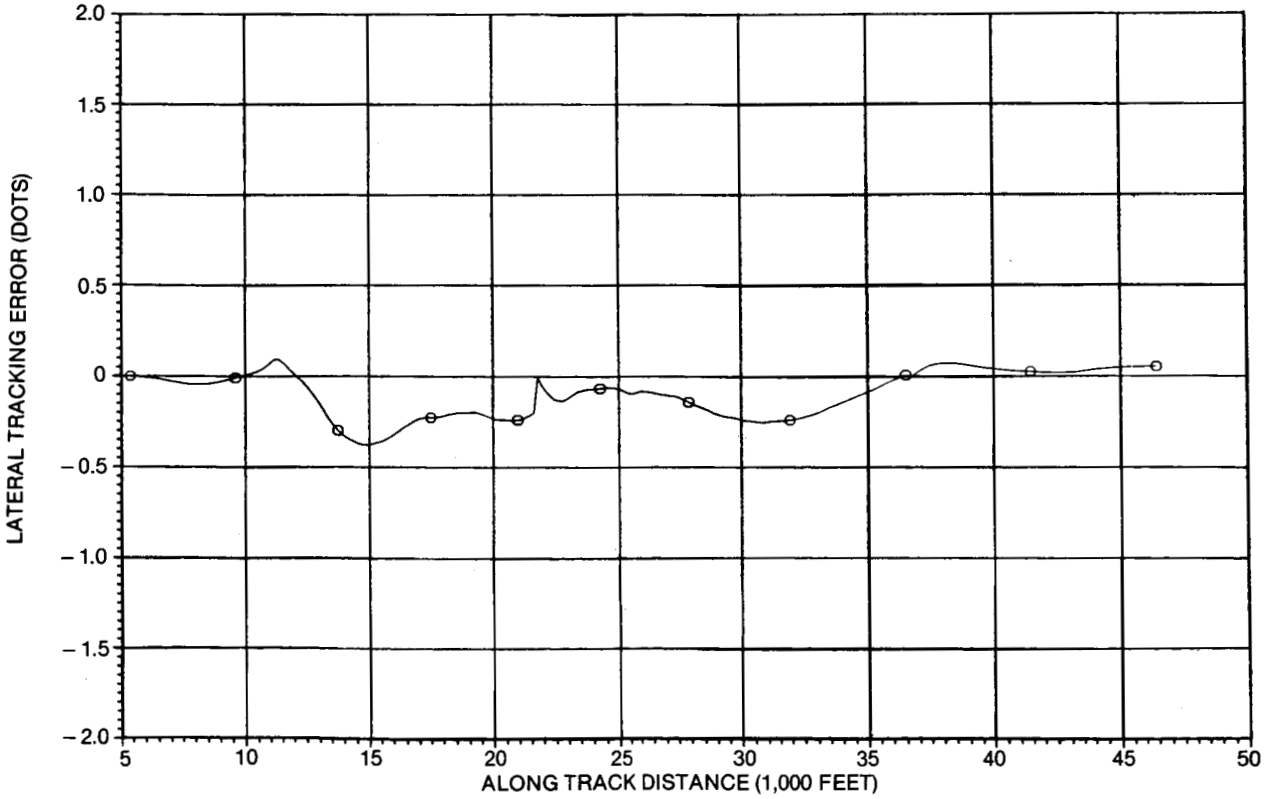

Figure 23. Lateral Tracking Error in Dots for Path 1 (Case 4)

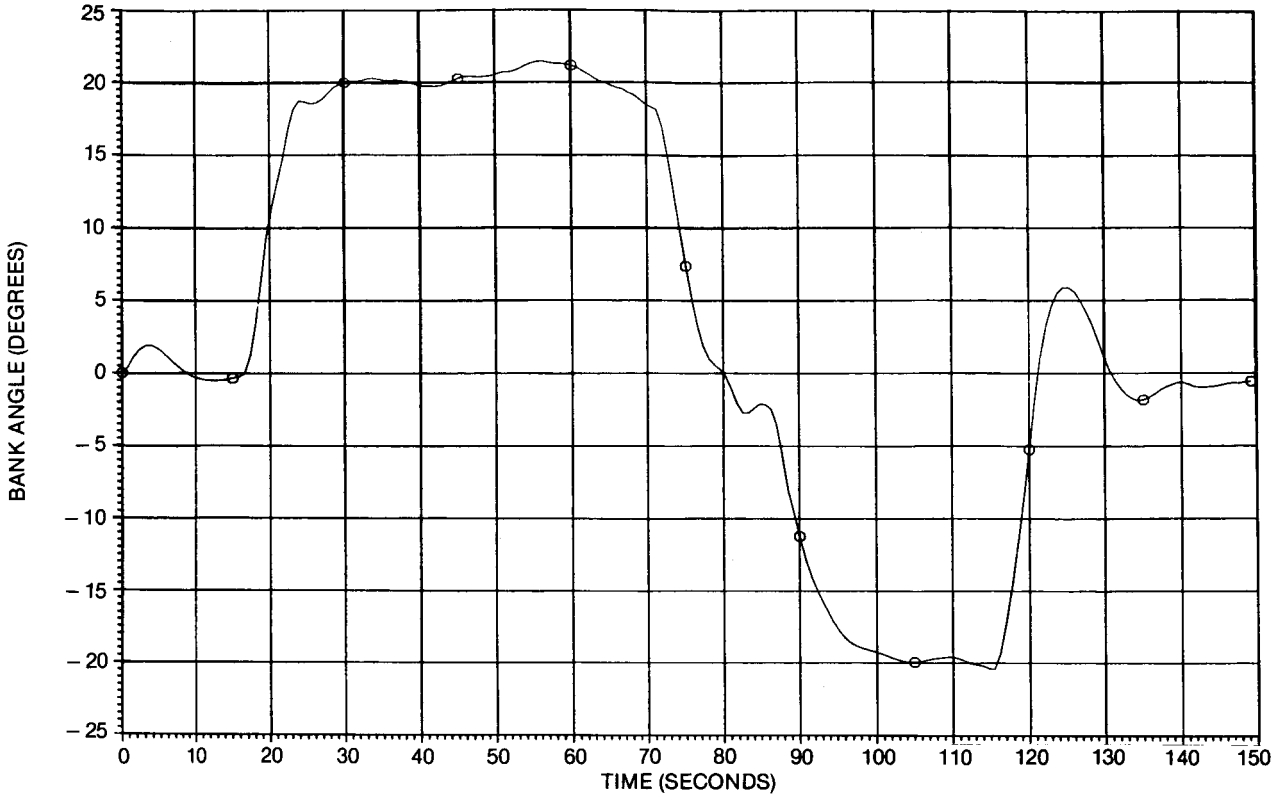

Figure 24A. Bank-Angle Time History for Path 2 (Case 5)

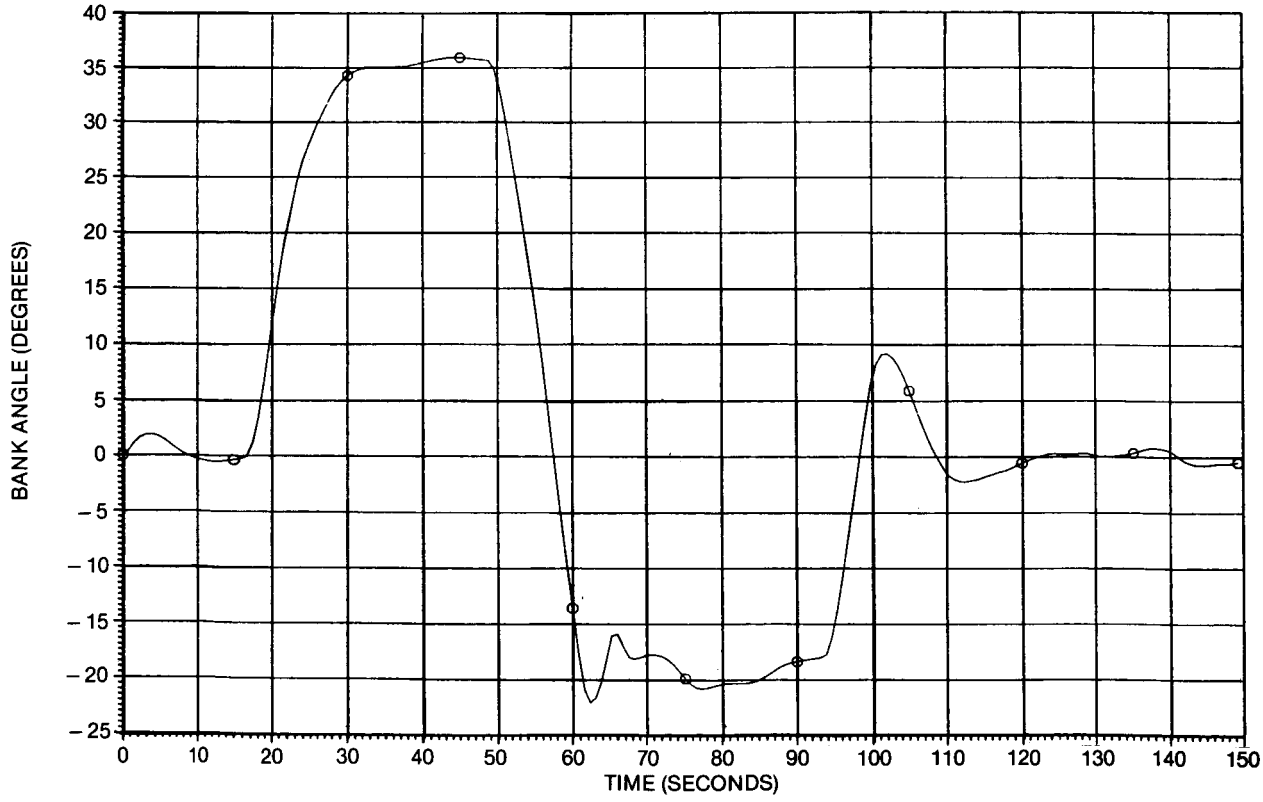

Figure 24B. Bank-Angle Time History for Path 3 (Case 6)

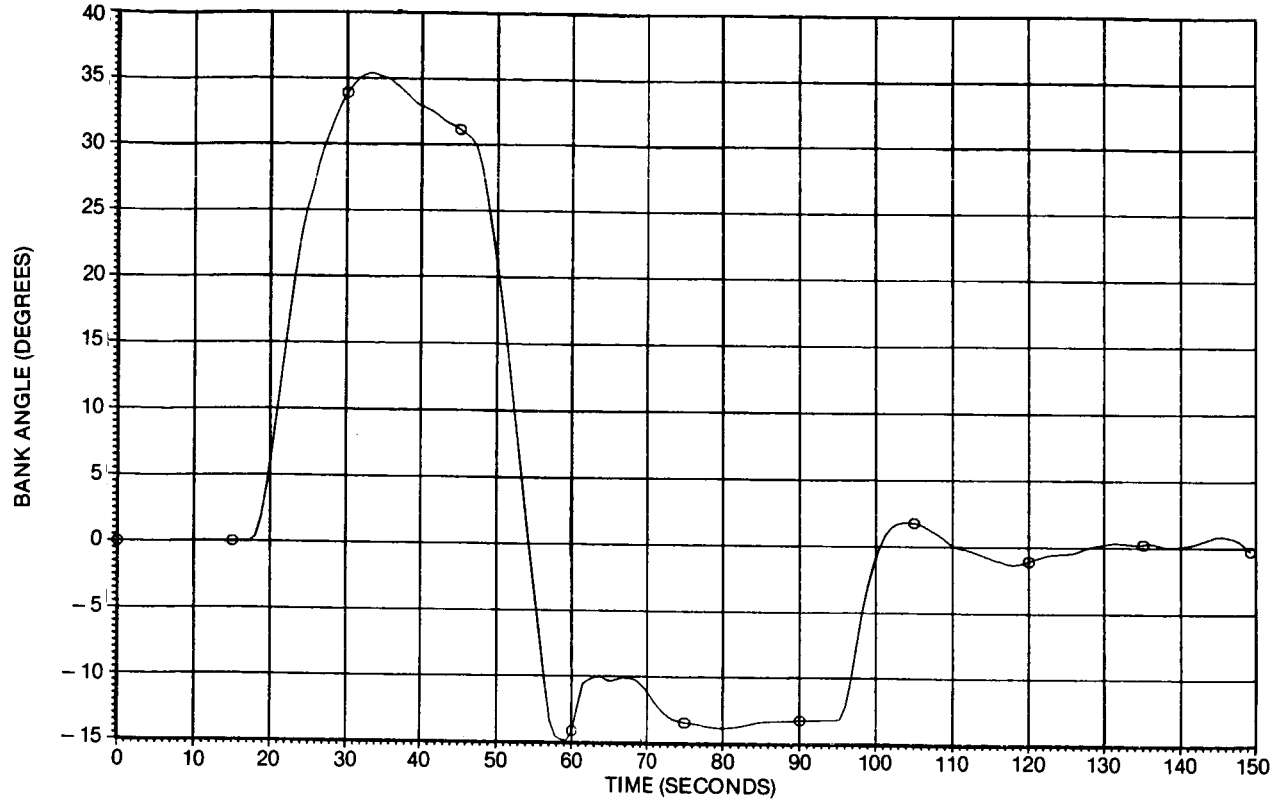

Figure 24C. Bank-Angle Time History for Path 4 (Case 7)

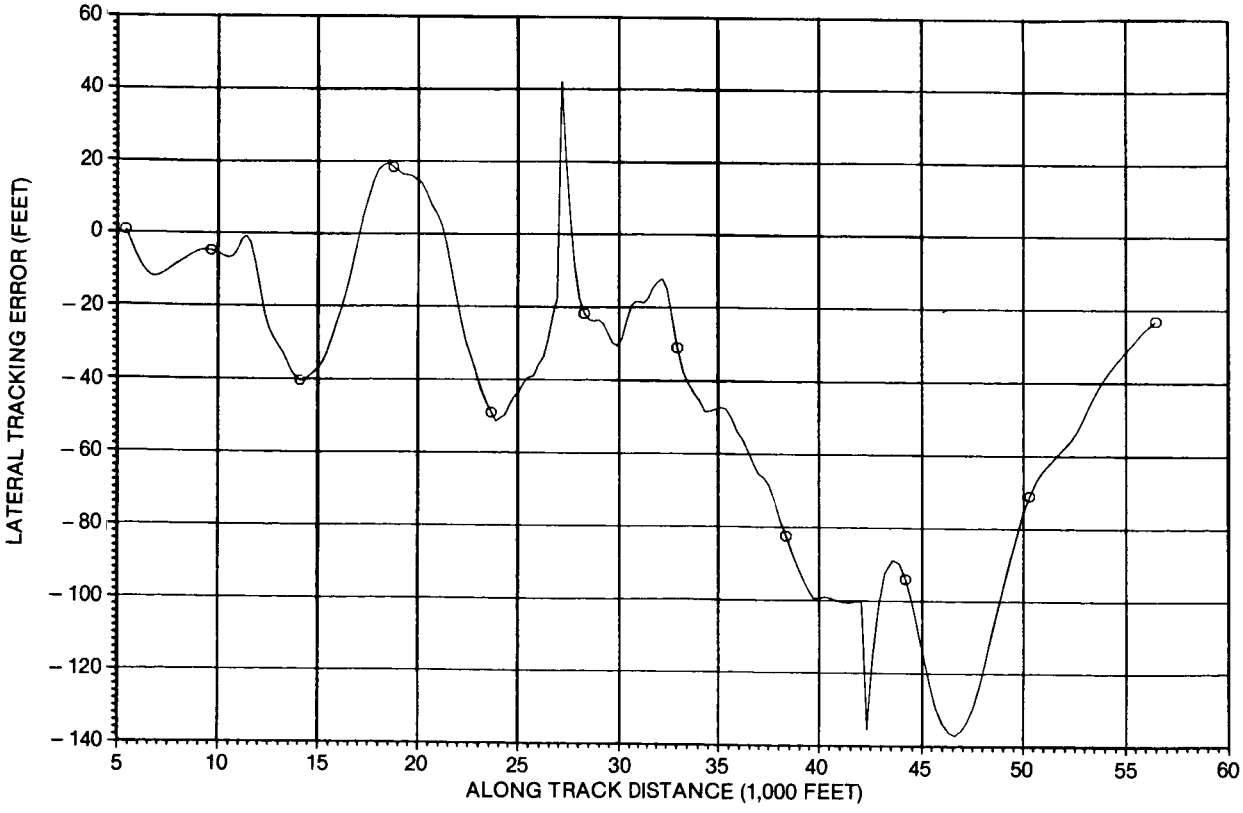

Figure 25A. Lateral Tracking Error for Path 2 (Case 5)

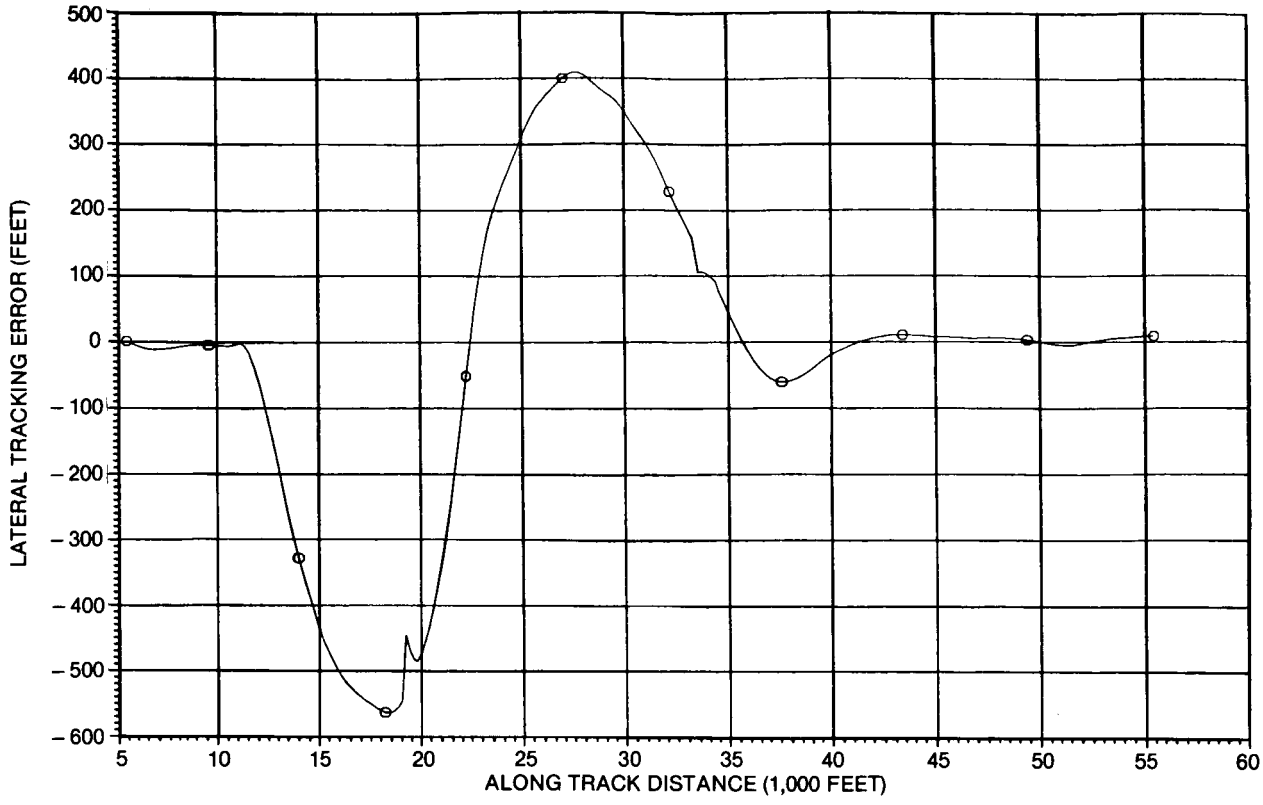

Figure 25B. Lateral Tracking Error for Path 3 (Case 6)

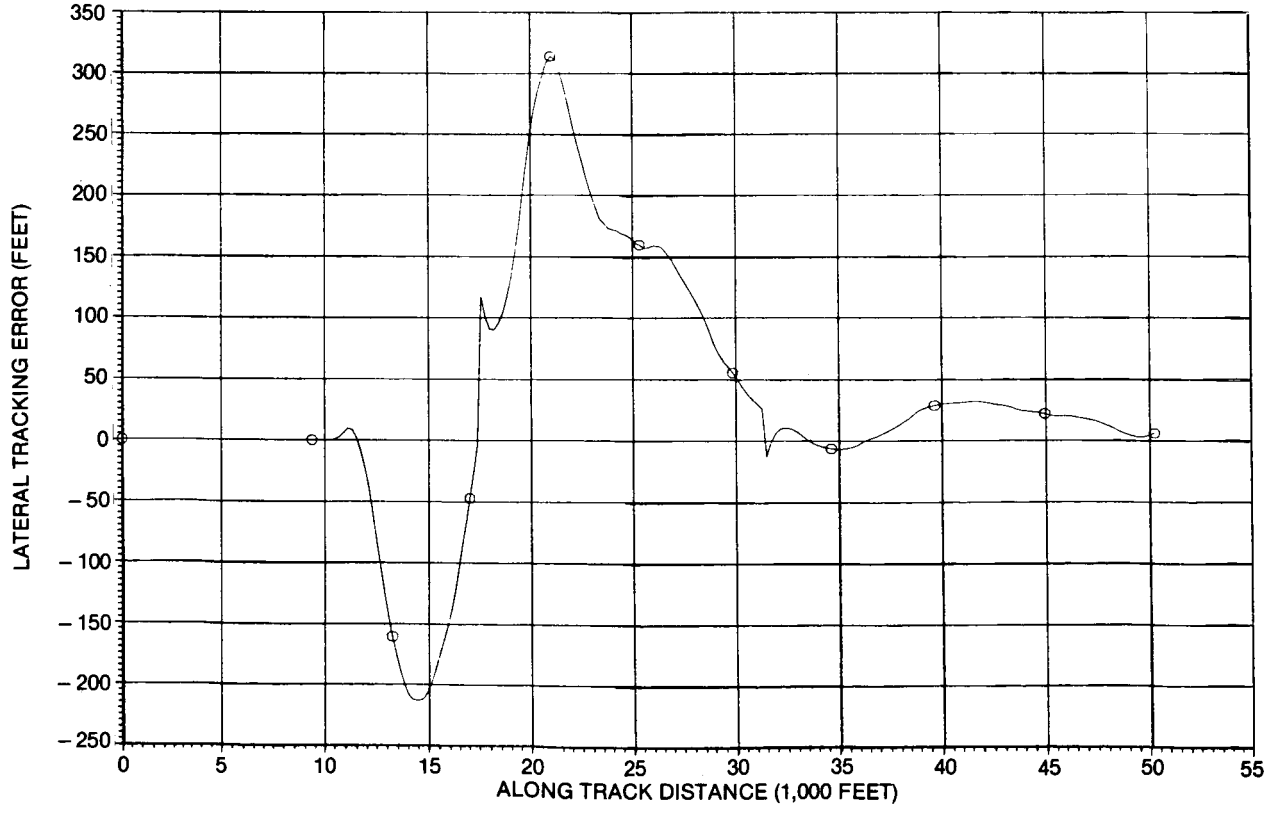

Figure 25C. Lateral Tracking Error for Path 4 (Case 7)

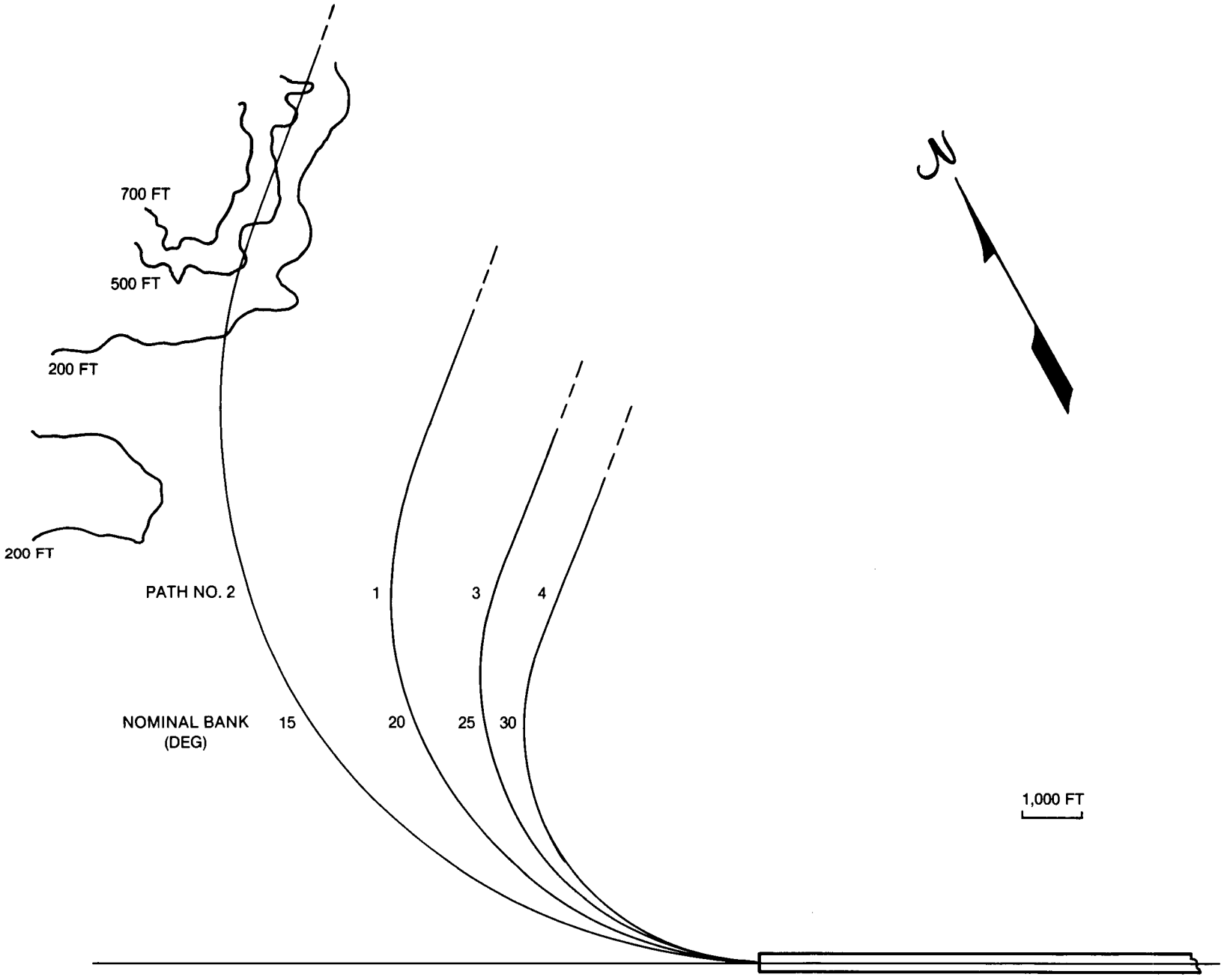

Figure 26. Ground Track for Paths 1, 2, 3, and 4

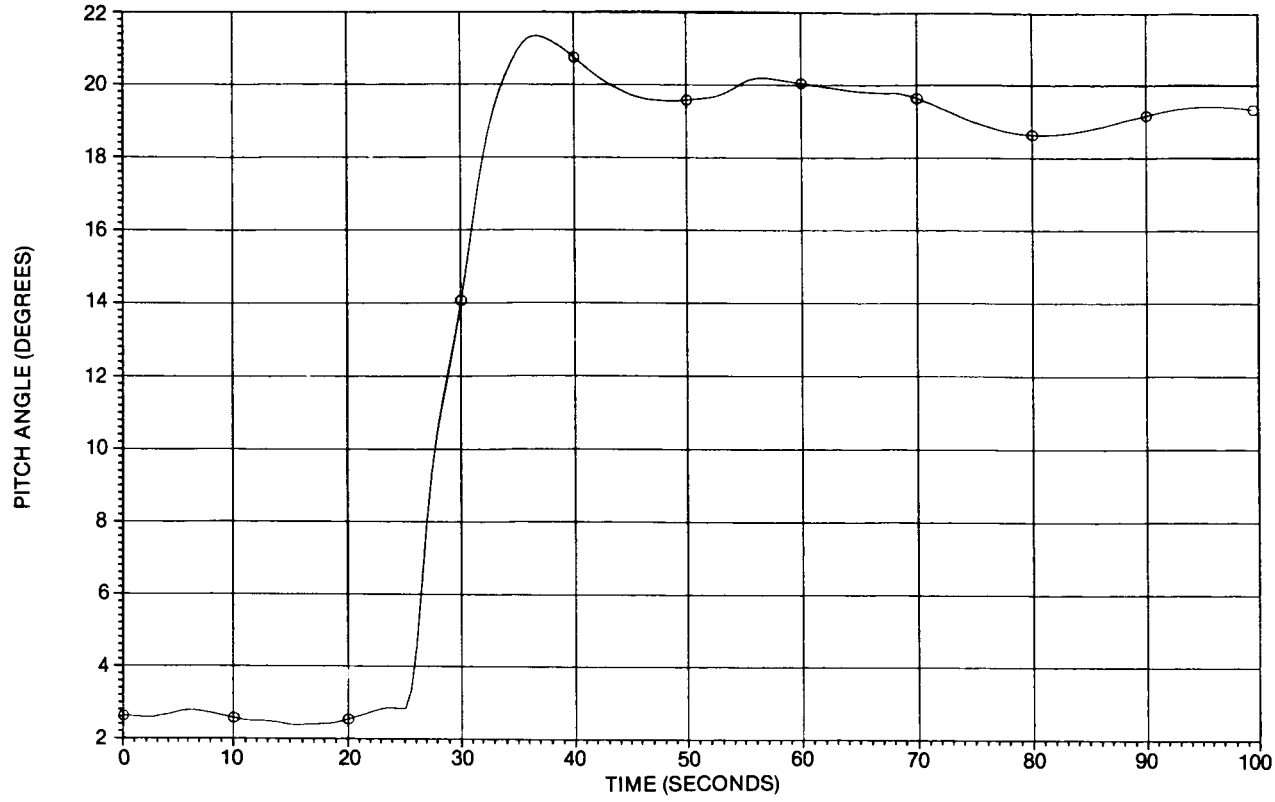

Figure 27. Pitch-Angle Time History (Case 8)

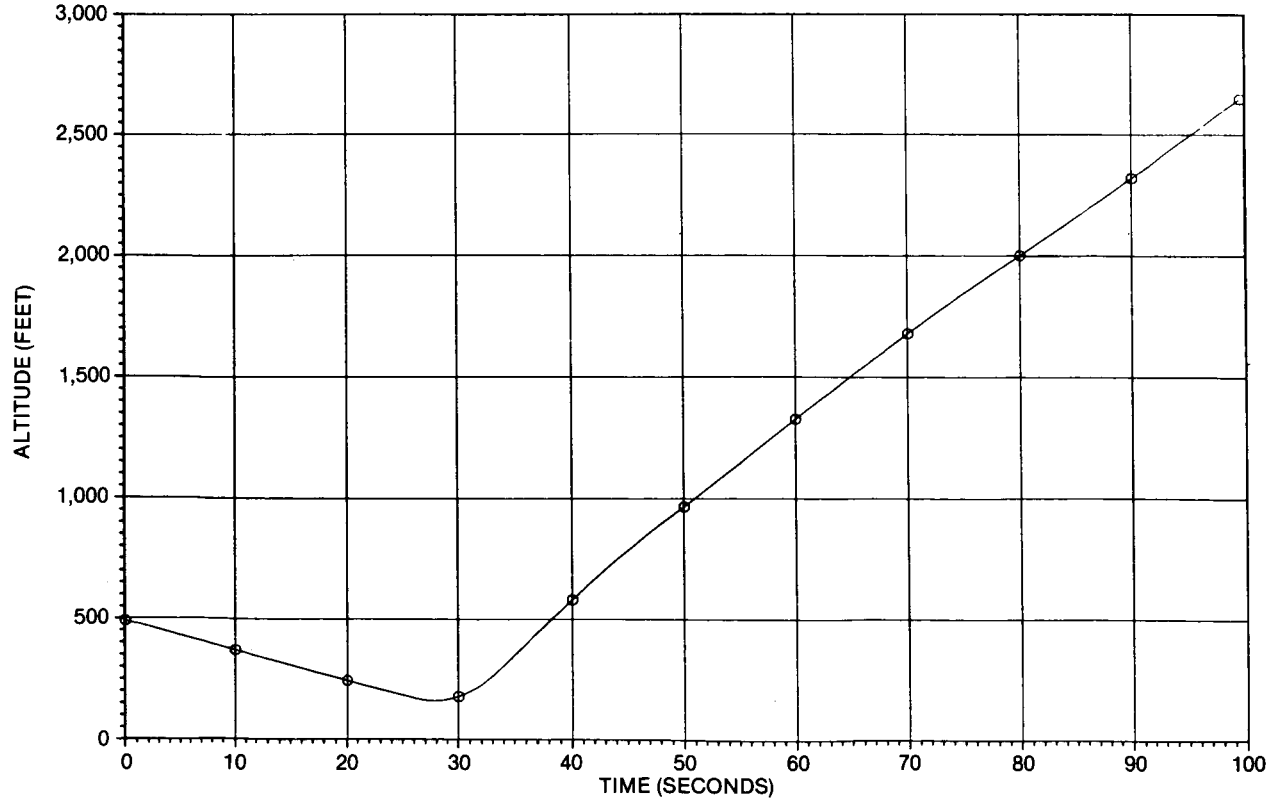

Figure 28. Altitude Time History (Case 8)

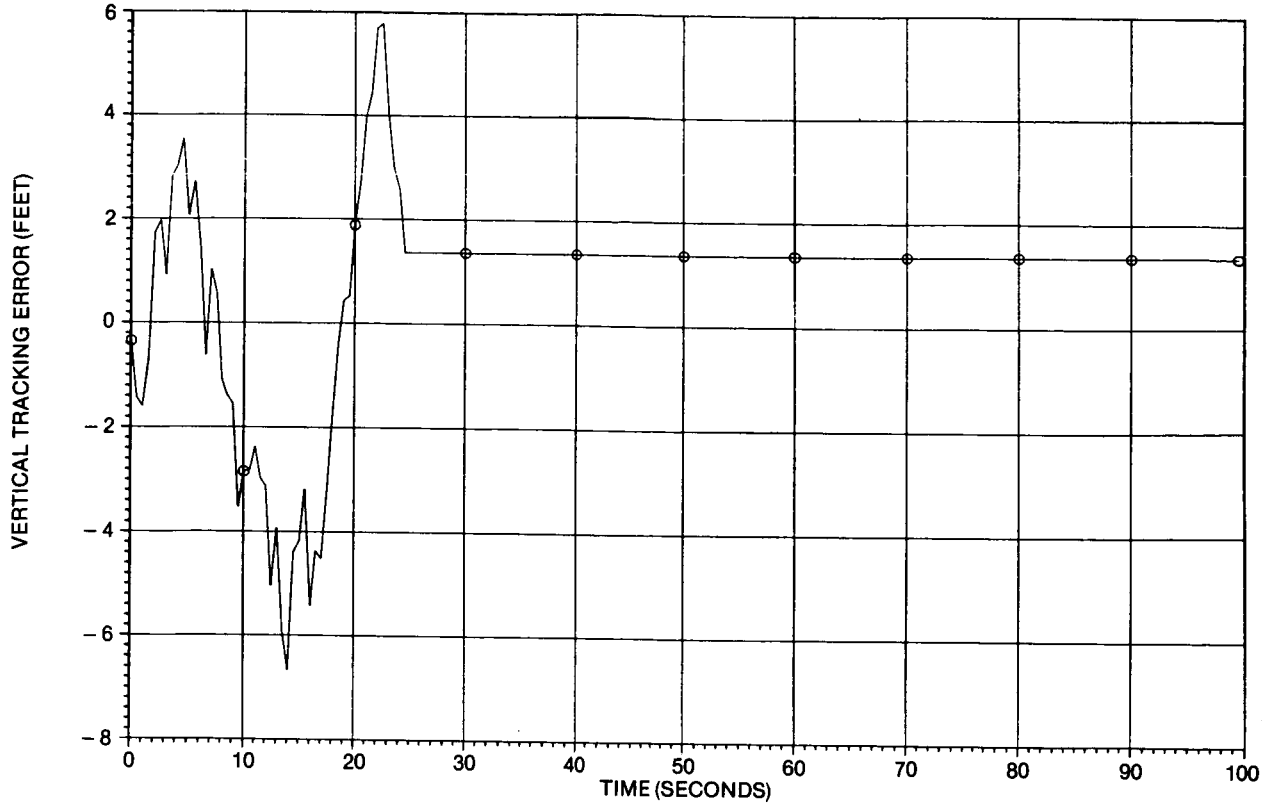

Figure 29. Vertical Tracking Error Time History (Case 8)

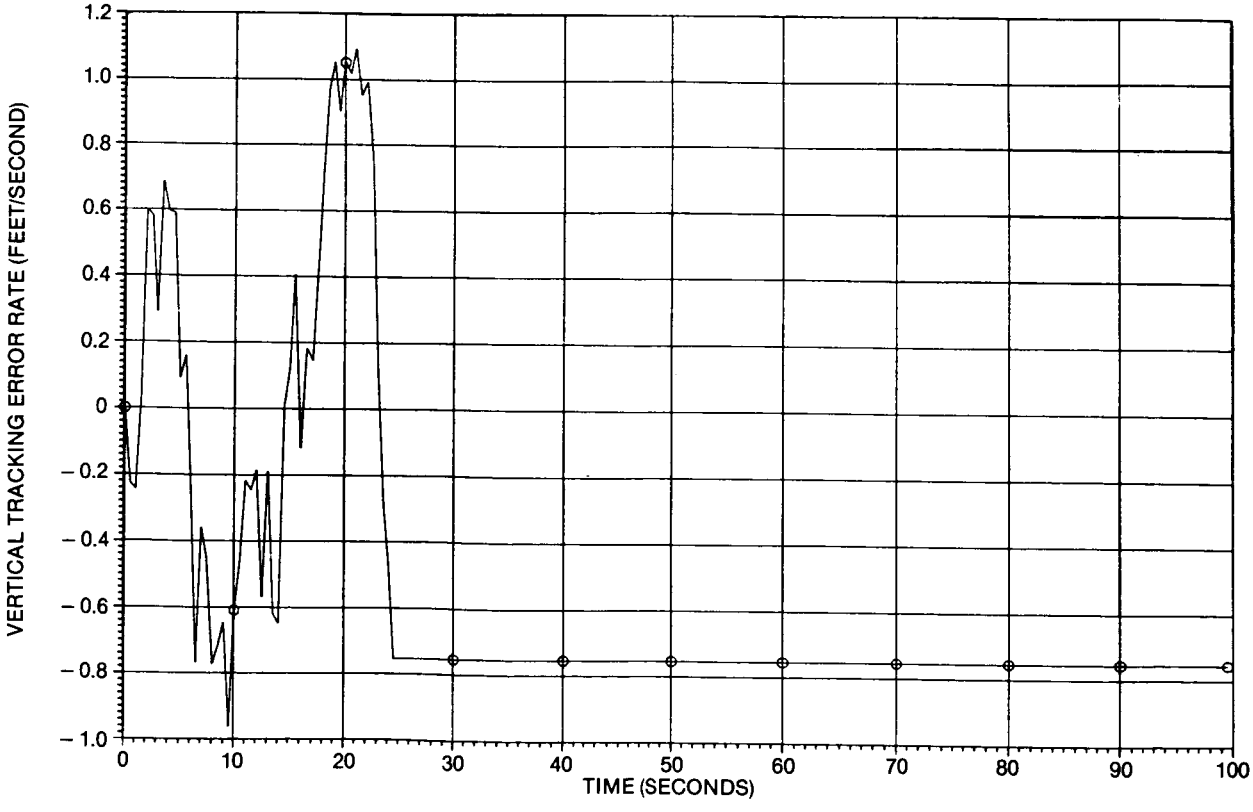

Figure 30. Vertical Tracking Error Rate (Case 8)

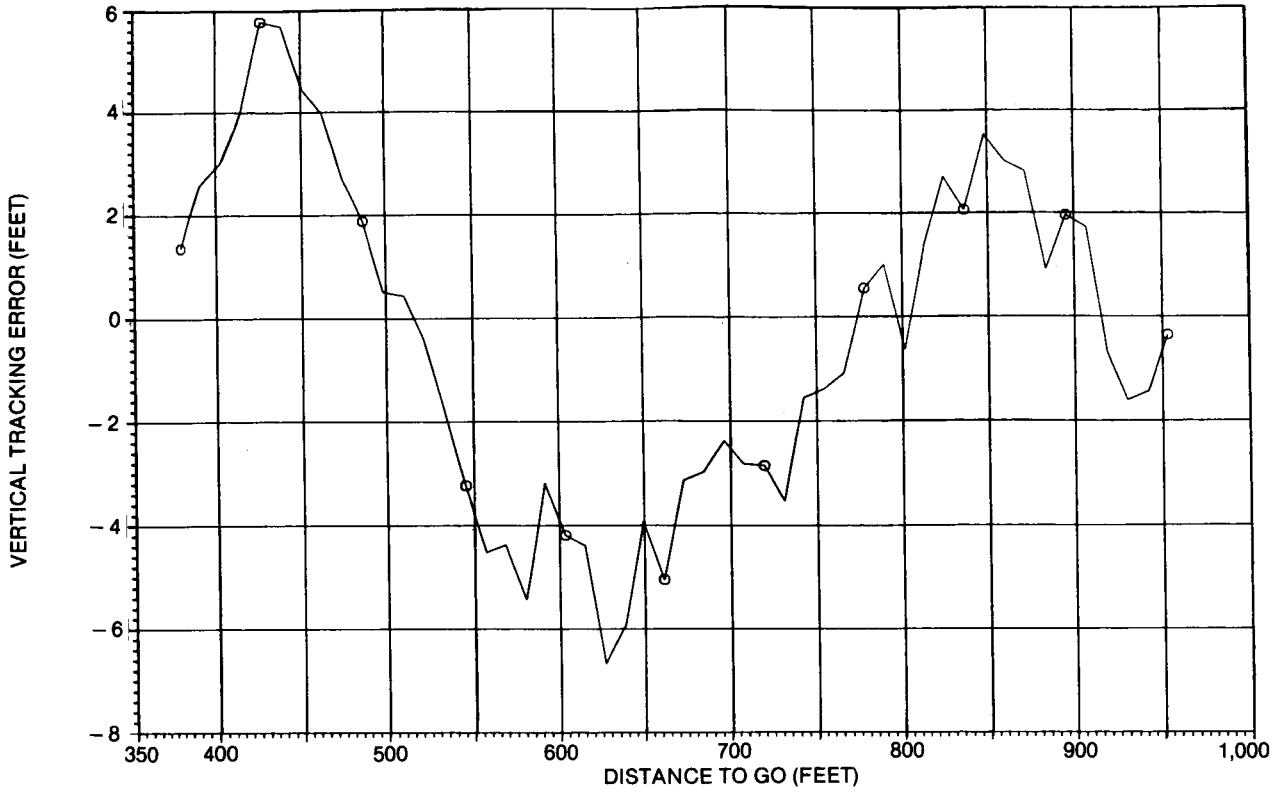

Figure 31. Vertical Tracking Error as a Function of Distance to Go (Case 8)

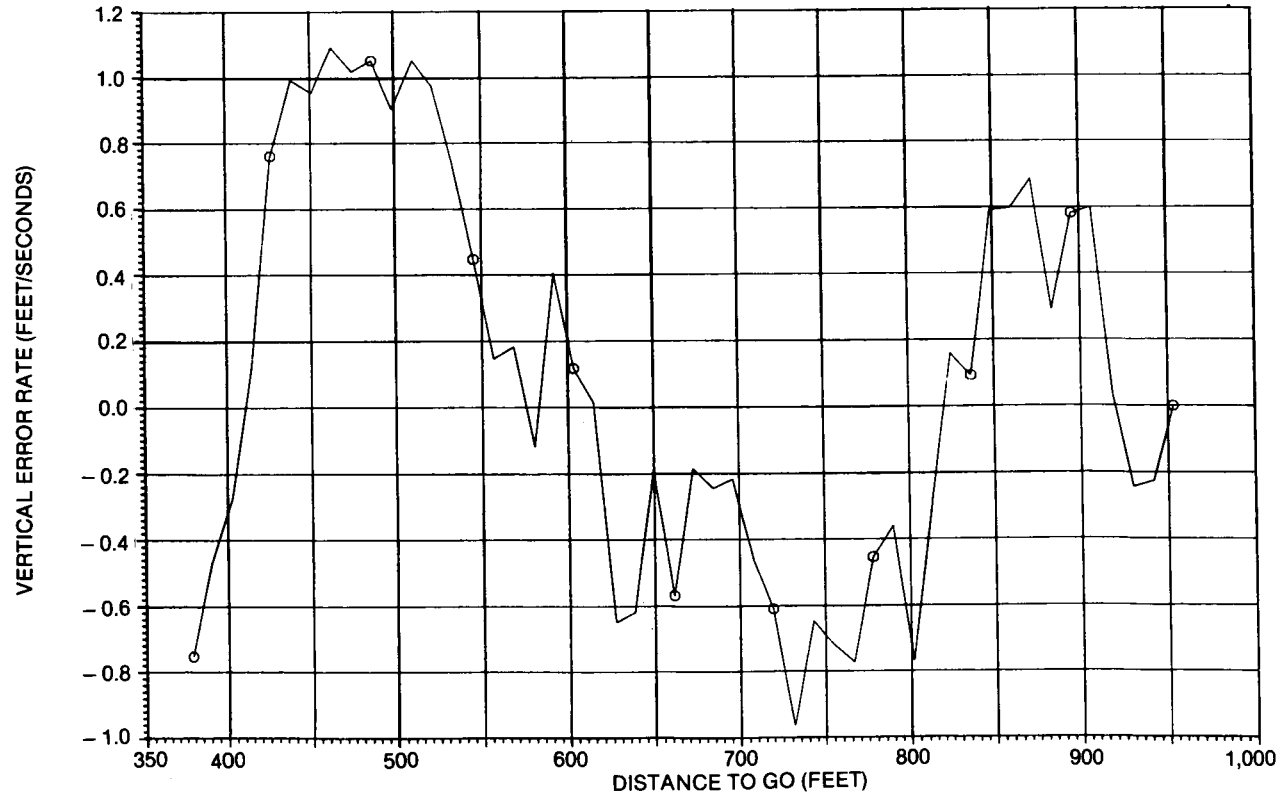

Figure 32. Vertical Tracking Error Rate as a Function of Distance to Go (Case 8)

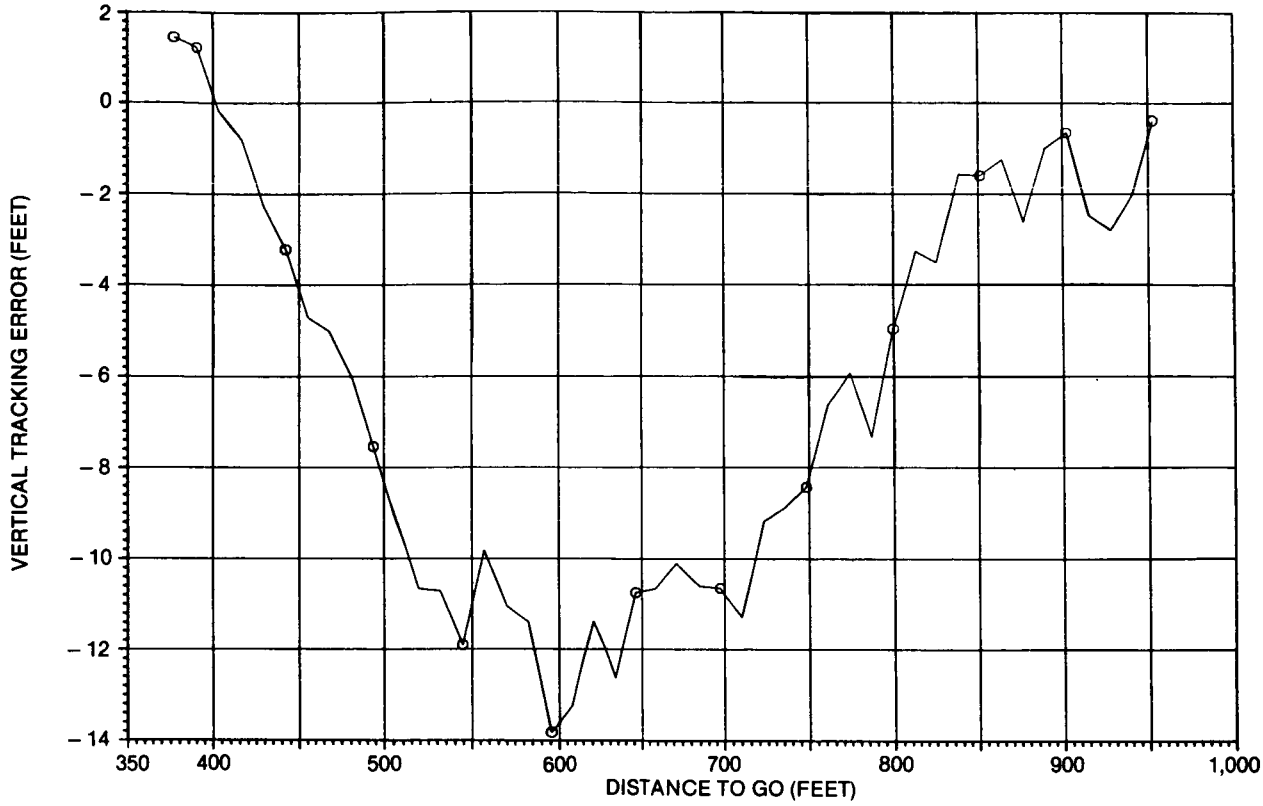

Figure 33. Vertical Tracking Error as a Function of Distance to Go (Case 9)

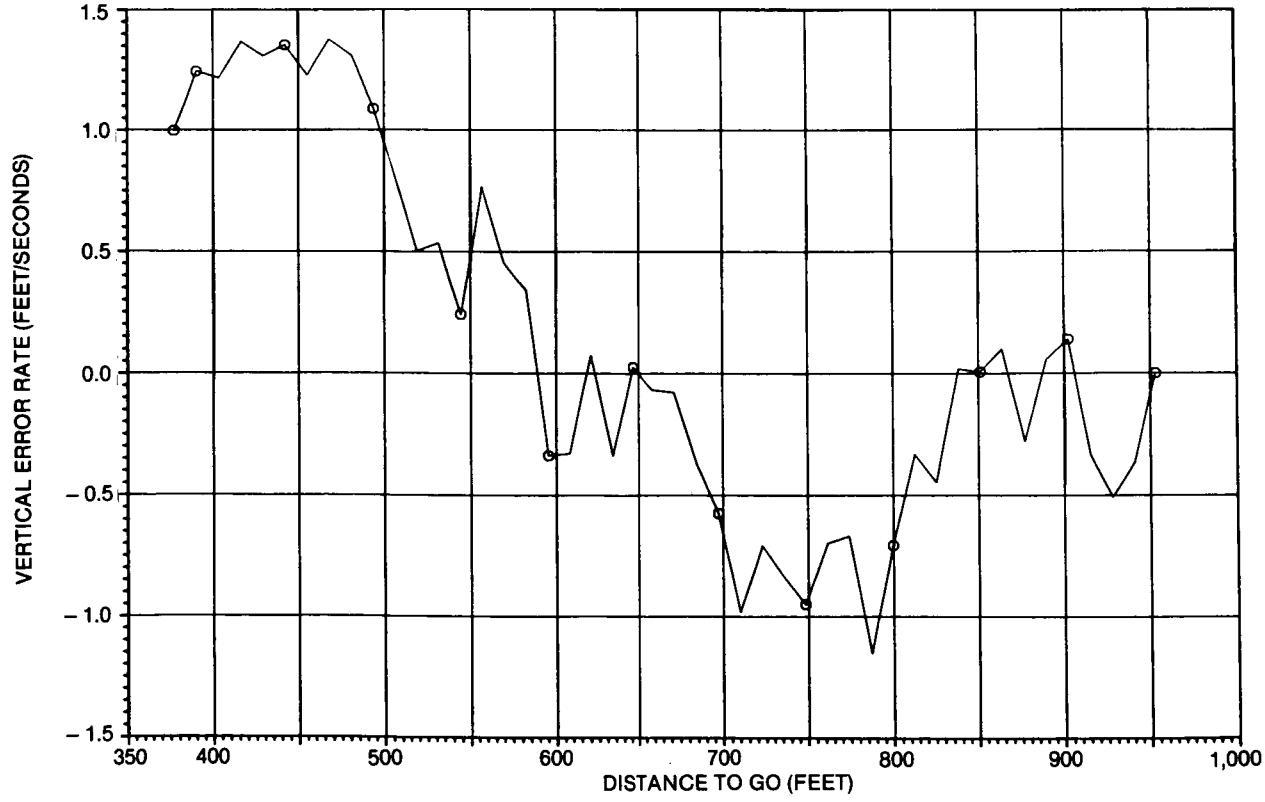

Figure 34. Vertical Tracking Error Rate as a Function of Distance to Go (Case 9)

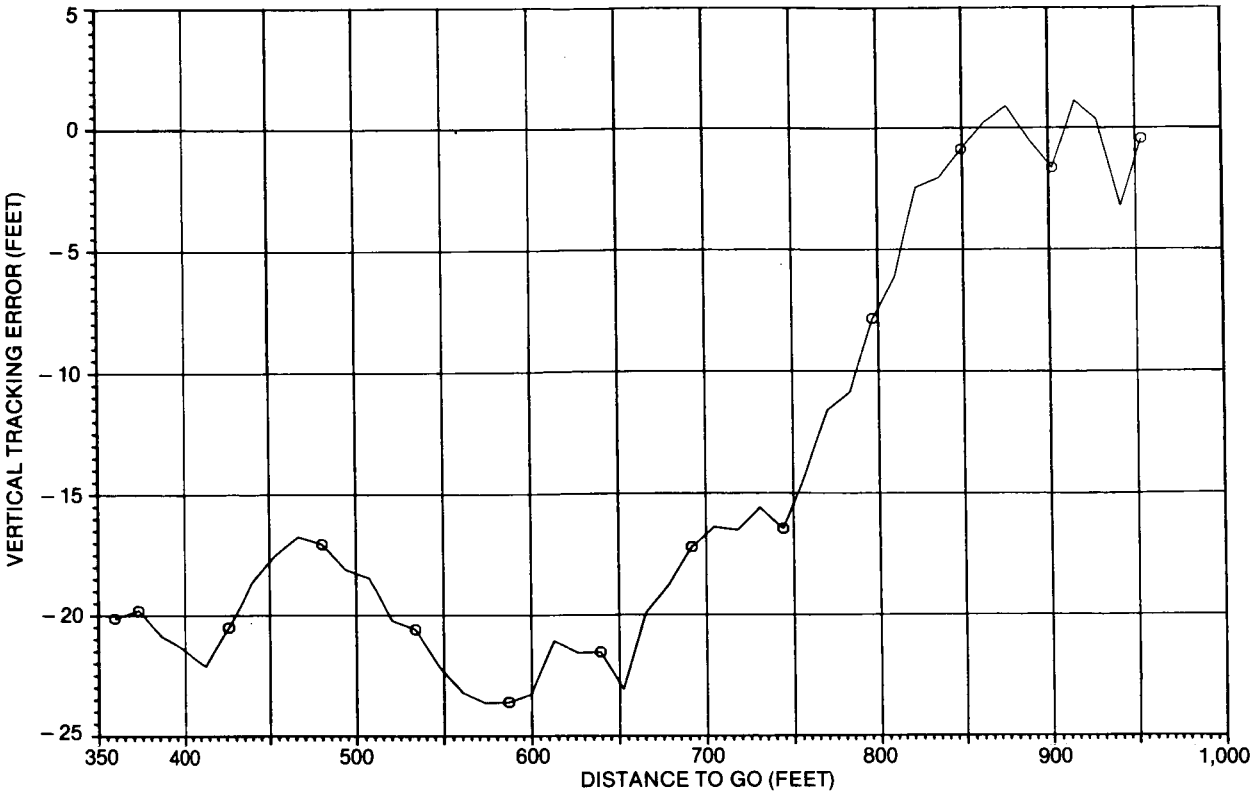

Figure 35. Vertical Tracking Error as a Function of Distance to Go (Case 10)

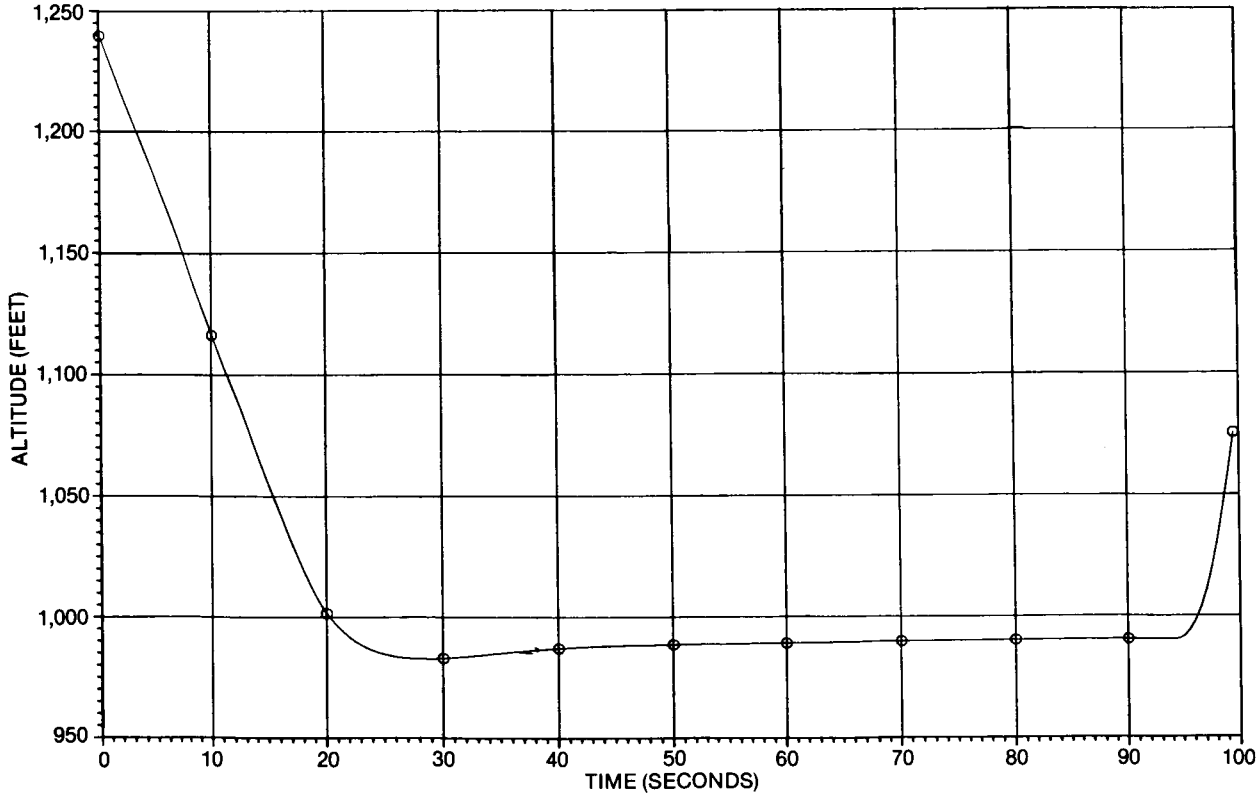

Figure 36. Altitude Time History (Case 11)

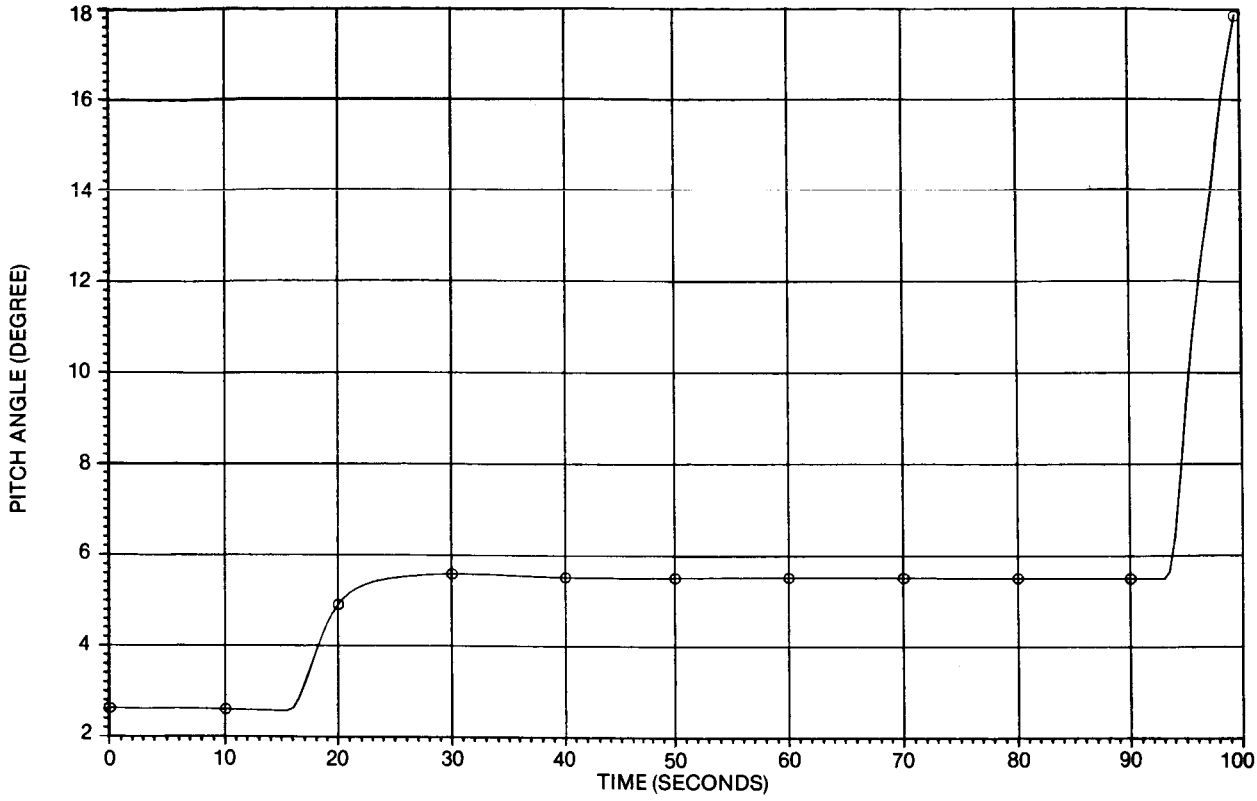

Figure 37. Pitch-Angle Time History (Case 11)

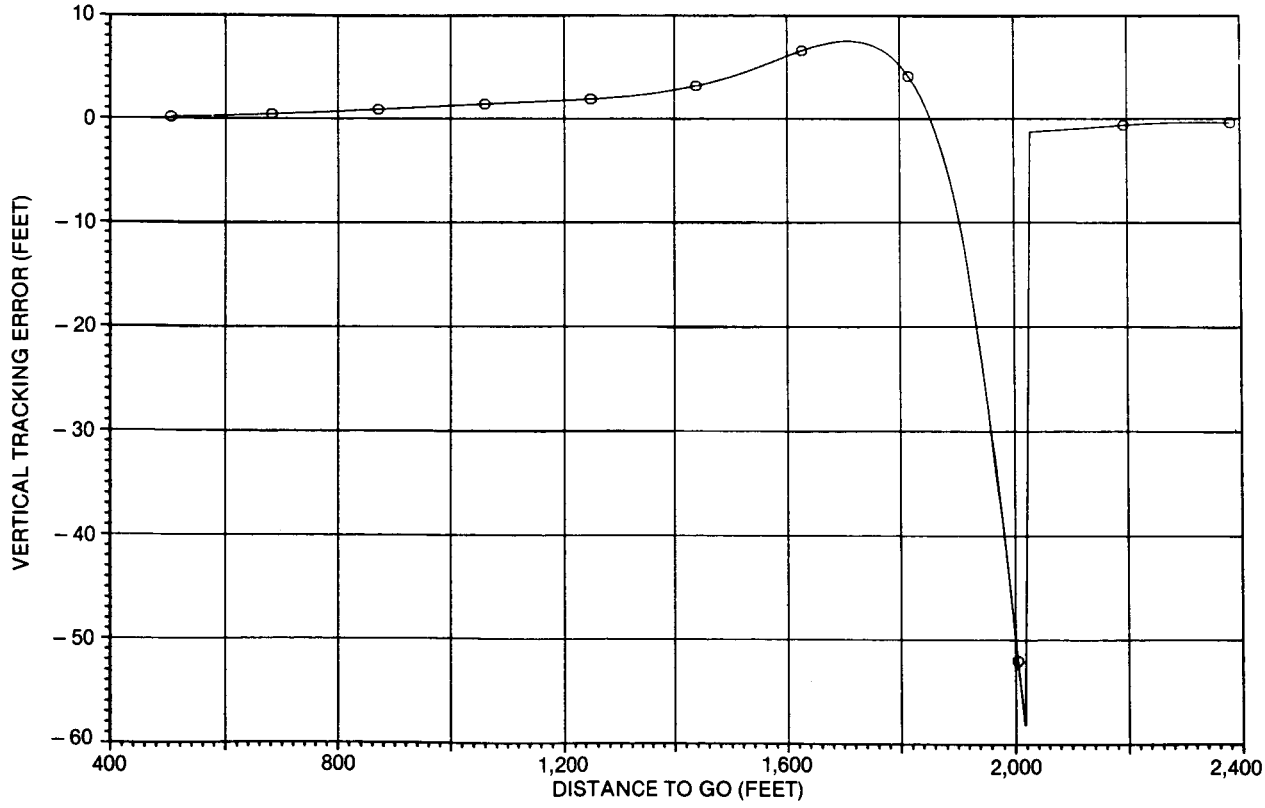

Figure 38. Vertical Tracking Error as a Function of Distance to Go (Case 11)

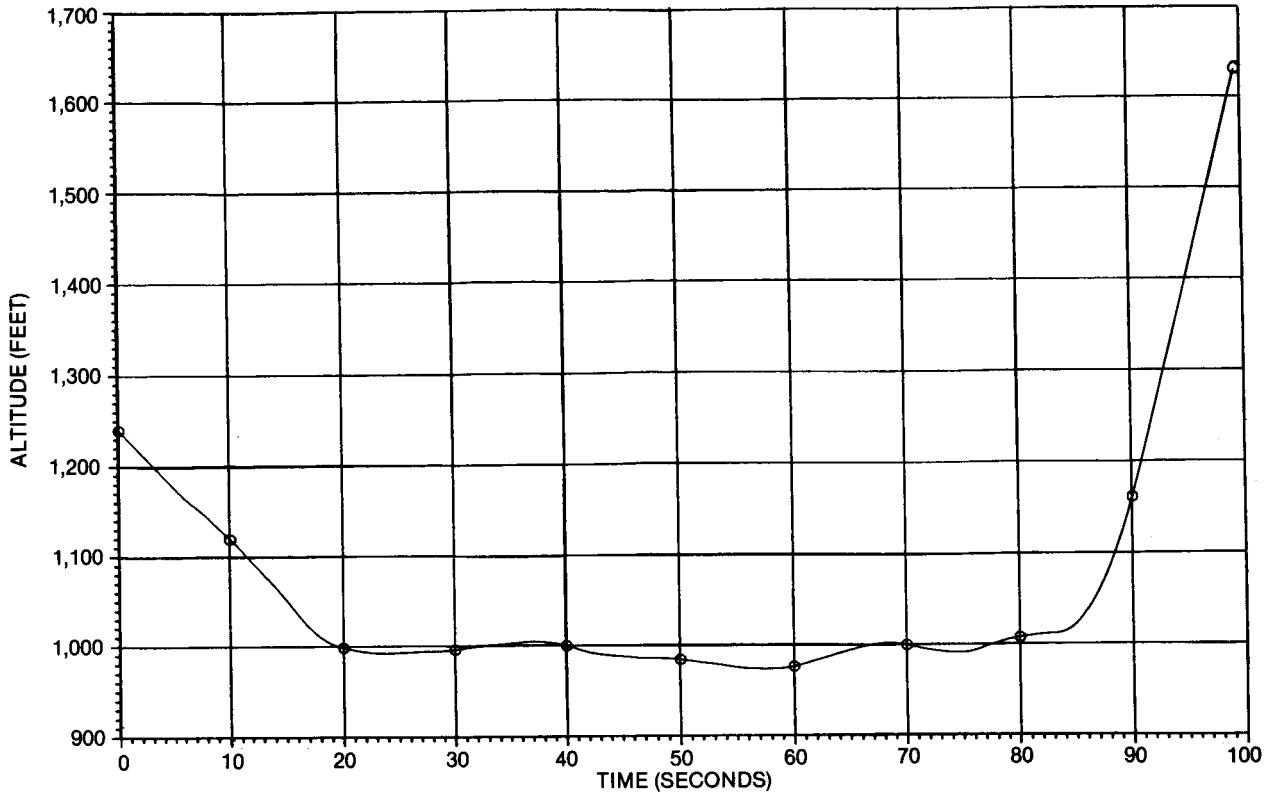

Figure 39. Altitude Time History (Case 12)

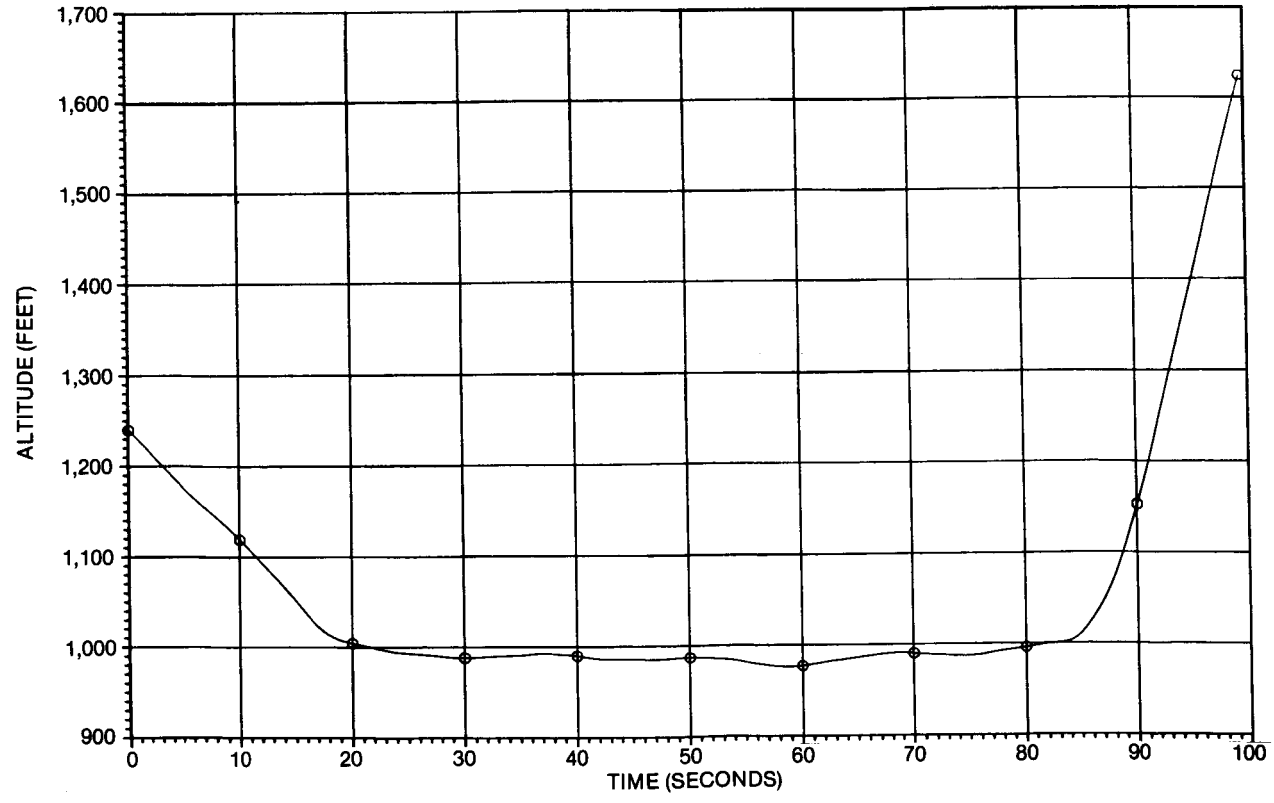

Figure 40. Altitude Time History (Case 13)

APPENDIX A - DERIVATION OF BACK AZIMUTH COORDINATES

From the geometry of Figure 1, one may write the following expression for the tangent of the azimuth angle, θ_{BAZ}:

$$\tan \theta_{BAZ} = \frac{-y'_m}{\left[z'^2_m + \left(x'_m - x_B\right)^2\right]^{1/2}} \tag{A1}$$

An expression containing the DME range is obtained from the triangle containing R_{DME} and z'_m:

$$R^2_{DME} - z'^2_m = y'^2_m + \left(x_D - x'_m\right)^2 \tag{A2}$$

Solve both (A1) and (A2) for $Y_m'^2$ and equate the results:

$$\text{From (A1):} \quad y_m'^2 = \left[z_m'^2 + \left(x_m' - x_B \right)^2 \right] \tan^2\theta_{BAZ} \tag{A3}$$

$$\text{From (A2):} \quad y_m'^2 = R_{DME}^2 - z_m'^2 - \left(x_D - x_m' \right)^2 \tag{A4}$$

Hence,

$$\left[z_m'^2 + \left(x_m' - x_B \right)^2 \right] \tan^2\theta_{BAZ} = R_{DME}^2 - z_m'^2 - \left(x_D - x_m' \right)^2 \tag{A5}$$

Expansion of (A5) will yield a quadratic in x_m'. Use of the following trigonometric identity will simplify the result:

$$1 + \tan^2\theta_{BAZ} = 1/\cos^2\theta_{BAZ}$$

Equation (A5) reduces to the form

$$x_m'^2 + bx_m' + c = 0 \tag{A6}$$

where b & c are defined by:

$$b = -2\left(x_B \sin^2\theta_{BAZ} + x_D \cos^2\theta_{BAZ} \right)$$

$$c = \left(x_B^2 + z_m'^2 \right) \sin^2\theta_{BAZ} + \left(x_D^2 + z_m'^2 - R_{DME}^2 \right) \cos^2\theta_{BAZ}$$

The above equations may be rewritten in terms of only one trig function:

$$b = -2\left[x_B + \cos^2\theta_{BAZ}\left(x_D - x_B\right)\right] \tag{A7}$$

$$c = \left(x_B^2 + z_m'^2\right) + \cos^2\theta_{BAZ}\left(x_D^2 - x_B^2 - R_{DME}^2\right) \tag{A8}$$

The solution to (A6) is

$$x_m' = -\frac{b}{2} \pm \sqrt{\left(\frac{b}{2}\right)^2 - c} \tag{A9}$$

and the expression for y_m' is obtained from (A3):

$$y_m' = -\left[z_m'^2 + \left(x_m' - x_B\right)^2\right]^{1/2} \tan\theta_{BAZ} \tag{A10}$$

The value for z_m' must be supplied from a source external to the MLS back azimuth equipment.

In implementing (A9) for x_m', one must determine the proper sign on the radical. For the geometry assumed here, the sign will be negative for an aircraft on approach (in front azimuth coverage). The sign switches when the quantity under the radical in (A9) passes through zero. Logic in the computer automatically selects the correct sign. It should be noted that the present study only contended with one switch of sign. However, in general, additional sign changes can occur depending on the aircraft position relative to the back azimuth and DME transmitters. More sophisticated logic would be required to account for the most general case.

APPENDIX B - WIND AND TURBULENCE MODELS

Included in the simulation are options for winds, whose magnitudes are a function of altitude, and for turbulence as additive terms to the winds. The factor that is a function of altitude is denoted W and is defined by

$$W = 0.43 \log h + 0.35$$

where h is the altitude in feet. Input values for S_x, S_y, and S_z (the wind magnitudes in knots) when the airplane is on the ground are used to compute the three wind components at altitude:

$$W_x = W\ S_x$$

$$W_y = W\ S_y$$

$$W_z = W\ S_z$$

The tail wind component S_x was simulated as 10 knots, and the cross wind S_y was +15 or -15 knots depending on the case. Value for S_z was assumed zero.

Turbulence is a random variable that may be added to the above winds. White noise is passed through first order filters whose parameters are functions of the wind components as shown in the following figure:

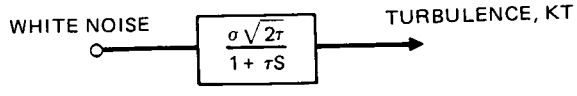

$\sigma_{WN} = 1.0$

FILTER PARAMETERS

	LONGITUDINAL	LATERAL	VERTICAL
τ(SEC)	$600/V_{TAS}$	$600/V_{TAS}$	$30/V_{TAS}$
σ(KT)	$0.15\ W_x$	$0.15\ W_y$	1.5

Outputs of the filters are denoted U_g, V_g, W_g and are used to form the total simulated winds:

$$W_{Tx} = W_x + u_g$$

$$W_{Ty} = W_y + V_g$$

$$W_{Tz} = W_z + W_g$$

APPENDIX C - MLS ANGLE AND RANGE NOISE

Angle and range signals as output from the MLS receiver will contain noise. For simulation purposes, additive noise has been included in the azimuth, elevation, and DME range variables θ_{AZ}, θ_{EL}, & R_{DME} respectively. The variables were modified to include this additive noise:

$$\theta_{AZ} = \theta_{AZ(TRUE)} + \theta_{AZ(NOISE)}$$

$$\theta_{EL} = \theta_{EL(TRUE)} + \theta_{EL(NOISE)}$$

$$R_{DME} = R_{DME(TRUE)} + R_{DME(NOISE)}$$

For purposes of simulation, white noise was shaped by filters to obtain the angle and range noise components. The figure below shows how these noise components were calculated (All cases in this study used these components):

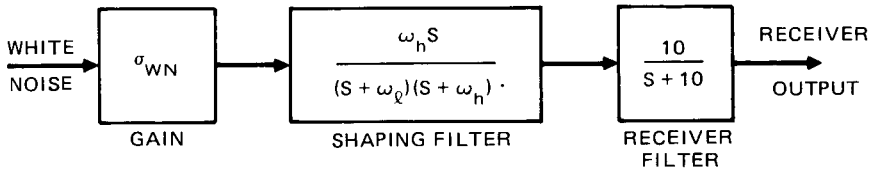

	AZIMUTH	ELEVATION	DME
ω_ℓ	= 0.001 RAD/SEC	= 0.001 RAD/SEC	= 0.001 RAD/SEC
ω_h	= 0.16 RAD/SEC	= 0.34 RAD/SEC	= 0.245 RAD/SEC
σ_{WN}	= 0.064	= 0.024	= 154.7
σ_{REC}	= 0.02 DEG	= 0.0097 DEG	= 53.4 FT

Standard Bibliographic Page

1. Report No.	2. Government Accession No.	3. Recipient's Catalog No.
NASA CR-178312		

4. Title and Subtitle	5. Report Date
SIMULATION OF AUTOMATIC PRECISION DEPARTURES AND MISSED APPROACHES USING THE MICROWAVE LANDING SYSTEM	JULY, 1987
	6. Performing Organization Code
7. Author(s)	8. Performing Organization Report No.
J. B. FEATHER	
9. Performing Organization Name and Address	10. Work Unit No.
DOUGLAS AIRCRAFT COMPANY 3855 LAKEWOOD BLVD. LONG BEACH, CA. 90846	
	11. Contract or Grant No.
	NAS1-16202
12. Sponsoring Agency Name and Address	13. Type of Report and Period Covered
NATIONAL AERONAUTICS AND SPACE ADMINSTRATION WASHINGTON, D.C. 20546	CONTRACTOR REPORT
	14. Sponsoring Agency Code

15. Supplementary Notes

LANGLEY TECHNICAL MONITOR: C. R. SPITZER
FAA TECHNICAL MONITOR: W. F. WHITE

16. Abstract

This report presents results of simulated precision departures and missed approaches using MLS guidance concepts. The study was conducted under the Terminal Configured Vehicle (TCV) Program, and is an extension of previous work by DAC in 1986 under the Advanced Transport Operating System (ATOPS) Technology Studies Program, contract NAS1-18028.

The study model included simulation of an MD-80 aircraft, an autopilot, and a MLS guidance computer that provided lateral and vertical steering commands. Precision departures were evaluated for San Francisco runway 28R using a noise abatement procedure. Several curved path departures were simulated with MLS noise and under various environmental conditions. Missed approaches were considered for the same runway, where lateral MLS guidance maintained the aircraft along the extended runway centerline. In both the departures and the missed approach cases, pitch autopilot take off and go around modes of operation were used in conjunction with MLS lateral guidance.

17. Key Words (Suggested by Authors(s))	18. Distribution Statement
MICROWAVE LANDING SYSTEM (MLS) PRECISION DEPARTURE GUIDANCE MISSED APPROACH GUIDANCE	UNCLASSIFIED - UNLIMITED

19. Security Classif.(of this report)	20. Security Classif.(of this page)	21. No. of Pages	22. Price
UNCLASSIFIED	UNCLASSIFIED	66	

For sale by the National Technical Information Service, Springfield, Virginia 22161

NASA Langley Form 63 (June 1985)